Research Square

Preprints are preliminary reports that have not undergone peer review. They should not be considered conclusive, used to inform clinical practice, or referenced by the media as validated information.

Characterization of pharmacological inhibition of the hERG potassium channel by nitazene opioids

Monisha R Chowdhury
University of Bristol

Matteo Baque
University of La Rochelle University Institute of Technology La Rochelle: La Rochelle Universite Institut Universitaire de Technologie

Thomas Osborne
University of Bristol

Hongwei Cheng
University of Bristol

Oliver Hannington
University of Bristol

Yihong Zhang
University of Bristol

Aziza El Harchi
University of Bristol

Caroline Copeland
King's College London

Robin A Corey
University of Bristol

Stephen C Harmer
University of Bristol

Jules Hancox
jules.hancox@bristol.ac.uk

University of Bristol https://orcid.org/0000-0002-2055-6482

Research Article

Keywords: brorphine, etonitazene, hERG, isotonitazene, metonitazene, nitazene, patch clamp, potassium channel, protonitazene, QT interval

Posted Date: October 21st, 2026

DOI: https://doi.org/10.21203/rs.3.rs-11234286/v1

License: This work is licensed under a Creative Commons Attribution 4.0 International License.
Read Full License

Characterization of pharmacological inhibition of the hERG potassium channel by nitazene opioids

By

Monisha R Chowdhury[1], Mattéo Baqué[1,2], Thomas Osborne[4], Hongwei Cheng[1], Oliver Hanington[1], Yihong Zhang[1], Aziza El Harchi[1], Caroline Copeland[3], Robin A Corey[4], Stephen C Harmer[1], Jules C Hancox[1*]

[1]Bristol Medical School, Biomedical Sciences Building, University Walk, Bristol, BS8 1TD.

[2]Departement Genie Biologique, IUT, La Rochelle Université, Rue Albert Einstein, BP 33060 – 17031 La Rochelle.

[3]Centre for Pharmaceutical Medicine Research, Institute of Pharmaceutical Science, Kings College, London, SE1 9NH.

[4]School of Psychology and Neuroscience, Biomedical Sciences Building, University Walk, Bristol, BS8 1TD.

*** Corresponding Author: jules.hancox@bristol.ac.uk**

Abstract

Nitazene opioids are 'street' drugs, many of which are substantially more potent than heroin. They are linked to respiratory depression, but other adverse effects have not been widely investigated. Machine learning models have predicted that several nitazenes may interact with a major drug anti-target, the hERG cardiac potassium channel. This study was conducted to evaluate effects on hERG of isotonitazene, protonitazene, etonitazene, metonitazene and the related piperadine benzimidazoline brorphine. hERG-expressing HEK293 cells were studied using automated patch clamp. Using a standard +20 mV command (WT) hERG tail current (I_{hERG}) was acutely inhibited by all 5 compounds with IC_{50} values between 0.5 µM (protonitazene) and 1.32 µM (isotonitazene). Inhibition showed voltage- and time-dependence consistent with gating-dependent block. The IC_{50} values for I_{hERG} inhibition for inactivation-attenuated (N588K) hERG were 3.3-5.1 fold those for WT for protonitazene and isotonitazene. Mutations at S5 and S6 aromatic residues (F557, Y652, F656) affected both compounds, with a particularly marked influence of F656A (13-fold WT IC_{50} for isotonitazene and 73-fold for protonitazene). Neither isotonitazene nor protonitazene impaired hERG channel trafficking to the surface membrane. *In silico* docking and molecular dynamics simulations reproduced binding to canonical binding residues. Combining fentanyl with isotonitazene or protonitazene exacerbated block compared to each compound alone. Hypokalemia (1 mM $[K^+]_o$) increased the potency of isotonitazene but not protonitazene. In conclusion, hERG is a direct target for nitazene opioids.

Key words: brorphine; etonitazene; hERG; isotonitazene; metonitazene; nitazene; patch clamp; potassium channel; protonitazene; QT interval.

1. Introduction

Potassium channels encoded by the *human ether-à-go-go Related Gene* (*hERG*, alternative nomenclature *KCNH2*) play key roles in cardiac ventricular repolarization (1). *hERG* underpins the rapid delayed rectifier (I_{Kr}) channel (2;3); loss- and gain-of-function *hERG* mutations respectively reduce and augment $I_{Kr,}$ leading to subtypes of long- and short- QT syndromes (LQTS / SQTS) (1;4). Due to unique structural features, hERG channels can interact with numerous clinically used drugs: hERG is the major culprit in the acquired (drug-induced) form of LQTS and the associated arrhythmia *torsades de pointes* (TdP) (1;5). Consequently, novel drugs are routinely evaluated for any propensity to produce pharmacological inhibition of hERG channels (1;5).

Opioid drugs are widely used for the management of moderate to severe pain but, due to their addiction potential, development of opioid tolerance and difficulties in withdrawal, they are linked to opioid use disorder (6). Due to their psychotropic effect, opioids have also long been subject to illicit use; there is currently a global epidemic of opioid overdose and misuse which, in the USA at least, is primarily driven by the use of fentanyl and its relatives (7;8). While respiratory depression is the dominant acute health risk with opioid use, some reviews have noted a link between some opioids and QT interval prolongation/TdP (9;10). Thus, methadone has potential for QT prolongation and TdP at low concentrations, while tramadol and oxycodone carry some risk at high doses (9;10). Additionally, methadone, oxycodone and fentanyl can all inhibit hERG channel current (11-13).

In recent years, nitazene opioids have emerged as a new threat in the opioid crisis (14-18). Nitazenes (2-benzylbenzimidazoles) are highly potent synthetic mu (μ) opioid receptor agonists that were originally developed in the 1950s, but have never been deployed clinically because they are strongly linked to respiratory depression (14;15). Nitazenes are relatively easy and cheap to synthesize and are increasingly misrepresented as/contaminate other illicitly sold drugs, which can lead to unintended exposure, with a high risk of severe respiratory depression and death (14;15;19). While it is recognized that nitazene use is linked to fatalities, mortality is likely to be underestimated both because nitazenes are not routinely tested for and because they are unstable in post-mortem blood samples (20;21).

Although pharmacological effects of nitazenes beyond respiratory depression are relatively understudied, cardiac arrest with nitazene consumption has been observed (22) and preclinical experiments on zebrafish have demonstrated direct cardiotoxic effects of etazene (23). To date, no *in vitro* study has investigated whether nitazenes interact with the hERG potassium channel, though a propensity for this has been suggested from deployment of machine-learning-model (MLM) based tools (24). The nitazenes etonitazene, isotonitazene, metonitazene, protonitazene and the piperidine benzimidazolone ('orphine') brorphine have been predicted (though not yet experimentally demonstrated) to inhibit hERG (24). The present study was undertaken to determine experimentally whether or not these drugs inhibit hERG and to investigate the underlying nature and basis of any observed effects. Our findings demonstrate clearly that acute nitazene exposure results in inhibition of hERG channel current (I_{hERG}), while chronic exposure does not affect hERG channel trafficking to the cell surface membrane.

2. Methods

2.1 Cell line maintenance and hERG constructs

Human embryonic kidney 293 (HEK293) cells expressing wild-type (WT) hERG were donated by Dr Craig January, University of Wisconsin (25). The N588K, Y652A, F557L and F656A mutations to hERG1a have been previously used in our laboratory (e.g. (26-28)). N588K and F557L mutants were generated in our laboratory based on a template of wild-type (WT) hERG1a construct in a modified pcDNA3.0 vector (L15) using the QuikChange® II site- directed mutagenesis kit (Agilent Technologies) (29;30).

In brief, a pair of complementary oligonucleotide primers containing the mutation (forward primer sequence 5' CTCATGTGCACCTTAGCGCTCATCG 3' and reverse primer sequence 5' CGATGAGCGCTAAGGTGCACATGAG 3' for F557L and forward primer sequence 5' GCTGGCTGCACAAACTGGGCGACC 3' and reverse primer sequence 5' GGTCGCCCAGTTTGTGCAGCCAGC 3' for N588K), which were synthesized by Merck (Dorset, UK), was used in a PCR reaction (95 °C for 1 min, 60 °C for 1 min, 68 °C for 16 min for 18 cycles). A DpnI digest of the PCR mix was then performed for 1 h at 37 °C. Competent DH5α Escherichia coli (Invitrogen, Paisley, UK) were transformed using standard procedures. The mutations were confirmed by sequencing of the entire open reading frame (Eurofins MWG Operon, Ebersberg, Germany) (29).

The full length F557L sequence in L15 was subcloned into an inducible expression vector pcDNA5/FRT/TO™ (V6520-20, Invitrogen, UK) by In Fusion HD Cloning (Takara Bio USA), N588K in L15 was subcloned into pcDNA5/FRT/TO™ using HindIII and NotI restriction enzyme sites. Cell lines stably expressing tetracycline-inducible F557L and N588K hERG channels were then generated by cotransfection of each of plasmid with Flp-recombinase expression vector pOG44 (V6005-20, Thermo Fisher Scientific, UK) into the Flp-In™ T-REx™ 293 Cell Line (R78007, Thermo Fisher Scientific, UK) as described in (31). Hygromycin (H011, TOKU-E 100 µg/ml final concentration) and Blasticidin (ant-bl-1, Invivogen 15 µg/ml) were used for selection and maintainance of the stable cell lines.

2.2 Cell culture

Cells were maintained and passaged as described previously (26;28;29). Cells were cultured in T-75 flasks and used for experiments when they reached approximately 70-80% confluency. Cells were passaged every 3-4 days and used between passages 15-30.

2.3 Electrophysiological recordings

Whole-cell patch-clamp experiments were performed using the QPatch Compact platform (Sophion Bioscience). QPlate 8 recording plates (SB0201) were stored at 4 °C prior to use. Once a recording plate was opened it was kept at room temperature and used within a week. Currents were recorded using standard extracellular and intracellular solutions. The external Tyrode's solution for WT, N588K, Y652A and F557L contained (mM): 140 NaCl, 4 KCl, 2 $CaCl_2$, 1 $MgCl_2$, 10 glucose, and 5 HEPES, adjusted to pH 7.4 with NaOH. For experiments using F656A and WT control the solution contained 94 mM KCl (with NaCl concentration correspondingly reduced) (27;28). For experiments investigating hypokalaemic conditions, the external solution contained 1 mM KCl (with NaCl concentration correspondingly increased) (32). The intracellular solution contained (mM): 130 KCl, 1 $MgCl_2$, 5 EGTA, 5 MgATP, and 10 HEPES, adjusted to pH 7.4 with KOH. Recordings were performed at room temperature, with a sampling rate of 10–25 kHz and filtered at 3.33-8.33 kHz (depending on the protocol used).

For each recording, data were assessed against predefined quality control criteria before inclusion in the analysis. Recordings were accepted if peak tail current exceeded 300 pA, cell capacitance (Cslow) was greater than 8 pF, leak current at −80 mV was less than −300 pA, seal resistance (Rseal) exceeded 300 MΩ, and series resistance (Rs) was below 10 MΩ (Sophion Application Report).

2.4 Drug preparation

The drugs studied (isotonitazene, etonitazene, protonitazene, metonitazene and brorphine) were selected on the basis of prior MLM prediction of hERG interaction (24). Isotonitazene and protonitazene were selected for detailed study as isotonitazene was the first nitazene to be identified as a street drug in Europe (14;15) and protonitazene is a structural isomer of

isotonitazene and was predicted to have the strongest hERG action in MLM evaluation (24). All the compounds studied are controlled substances and were purchased from Cayman Chemical through Cambridge Biosciences, under a UK Home Office Schedule 1 Controlled Drugs licence. Nitazenes were prepared as stock solutions in DMSO and diluted to final concentrations in external solution on the day of the experiment. Drug stock solutions were made to make 1 to 30 mM and stored at -20°C. Quinidine gluconate (Sigma-Aldrich, Gillingham, UK) was dissolved in Milli-Q water to produce a stock solution of 10 mM and was diluted in Tyrode's solution for use. The final solvent concentration in external solutions to which cells were exposed did not exceed 0.1%.

2.5 Trafficking assay

Evaluation of the effects of isotonitazene and protonitazene on hERG channel trafficking was conducted as described previously ((26;33); see online supplement for more details).

2.6 Data Analysis

Raw traces were processed on Sophion Analyzer 8.0 (Sophion Biosciences, Denmark) and analysed using Microsoft Excel (Microsoft Corporation, USA), GraphPad Prism 10.4.2 (GraphPad Software Inc., USA) and Clampfit 10.7 (Molecular Devices, USA) with results expressed as mean ± SEM. Statistical comparisons were made using paired t-test, one-way and two-way repeated-measures ANOVA with Tukey post hoc test as appropriate. A p value <0.05 was considered statistically significant.

All nitazene compounds produced a steady state block after ~3-4 minutes of drug exposure at which point I_{hERG} was measured to observe the drugs inhibitory effects. The fractional block of different compounds at varying concentrations was determined by using the equation:

$$Fractional\ block = 1 - I_{drug}/I_{control} \qquad (1)$$

Where 'fractional block' represents the inhibition of I_{hERG} at a given concentration, $I_{control}$ represents the current before drug application and I_{drug} is the current after ~3-4 minutes of drug exposure.

The concentration–response relationship for I_{hERG} inhibition was analysed by fitting fractional block data with the Hill equation in order to determine IC_{50} and Hill slope (nH) values.

$$Fractional\ block = 1 / 1 + 10^{(logIC_{50} - X)\ n_H} \qquad (2)$$

Where 'fractional block' shows the inhibition of I_{hERG} at a given concentration, x represents the logarithm concentration, IC_{50} is the concentration producing half-maximal inhibition of I_{hERG}, and n_H is the Hill coefficient describing the steepness of the concentration–response curve.

Voltage-dependent activation of I_{hERG} was assessed from current–voltage relationships generated from tail currents and fitted with a Boltzmann function.

$$I = I_{max} / (1 + exp\ ((V_{0.5} - V_m)/k)) \qquad (3)$$

where I is the tail current amplitude measured following each test potential (V_m), I_{max} is the maximum tail current obtained during the protocol, $V_{0.5}$ is the membrane potential at which half-maximal activation occurred, and *k* is the slope factor describing the steepness of the activation curve.

Voltage dependence of I_{hERG} inactivation was assessed using the equation:

$$(I/I_{max}) = 1 - 1/ (1 + exp\ ((V_{0.5} - V_m)/k)) \qquad (4)$$

where I/I_{max} is the normalised current at a given membrane potential, V_m is the membrane potential, $V_{0.5}$ is the voltage at which inactivation is half maximal, and *k* is the slope factor describing the voltage dependence of inactivation. For inactivation data plots I_{hERG} transients were corrected for potential deactivation as described in (34).

2.7 In silico molecular docking and molecular dynamics

Docking poses for isotonitazene and protonitazene at hERG were generated using the GNINA docking platform (35), which employs a convolutional neural network (CNN) scoring function on top of the standard AutoDock Vina (36) methodology. Docking was performed against the Dickson pore model of hERG (37). Based on the 5VA1 structure, this model conserves the canonical pore architecture while representing an MD-derived conformation consistent with experimentally validated hERG blocker binding and mutagenesis data (37). The docking grid box was centred on residue F656, with dimensions of x=20 Å × y=20 Å × z=20 Å. Docking via GNINA yielded nine poses per molecule; the pose selected for simulation was that with the lowest variance among poses which also conserved the overall docking ensemble.

MD simulations were used to assess pore-residue interactions between the nitazene compounds and the stability of the hERG–nitazene complexes. Ligands were parameterised using the CHARMM-GUI Ligand Modeller, with the tertiary amine of each compound modelled in the protonated form, as predicted from pKa analysis (38). Parameterised ligands were aligned to their respective GNINA poses and embedded into a lipid bilayer using CHARMM-GUI Membrane Builder (39;40). Each bilayer comprised a 4:1 ratio of 1-palmitoyl-2-oleoyl-sn-glycero-3-phosphocholine (POPC) to cholesterol, solvated with TIP3P water and neutralised with KCl at 0.15 M. Protein side chains were assigned default protonation states, based on pKa analysis using propKa 3.1 (41).

Systems were minimised and equilibrated locally using GROMACS following the standard CHARMM-GUI protocol (42;43). Following equilibration, production simulations were run with a 2 fs timestep for 5 runs of 500 ns per run, using Parrinello–Rahman pressure coupling (semi-isotropic, reference pressure 1 bar, τ_P = 5.0 ps, compressibility = 4.5×10^{-5} bar^{-1}) and Nosé–Hoover temperature coupling (τ_T = 1.0 ps) maintaining system at 303.15 K.

Binding free energies were estimated using gmx_MMPBSA for the isotonitazene and protonitazene systems (44). Prior to analysis, gmx trjconv was used to centre trajectories and fit them to the protein and ligand coordinates, removing rotational and translational motion. The protein and ligand groups were then indexed together to define a single complex group required for the MM-PBSA calculation. Gmx_MMPBSA v1.5.0 requires GROMACS 2019.2-format run input, gmx grompp was used to regenerate tpr files in this version prior to submission.

Analyses were performed over frames 50–550 of the production trajectory at a temperature of 303.15 K. These were chosen to unbias unstable docking poses. Given that the target is a membrane-embedded ion channel, membrane-specific Poisson-Boltzmann settings were applied (memopt=2), with a membrane dielectric of 4.0, solute dielectric of 10.0, membrane thickness of 40 Å centred at z = 62, and a single-pore geometry (poretype=1) (45). The CHARMM-specific radii set (PBRadii=7, charmm_radii) was used in accordance with the CHARMM36m force field used to parameterise the system, and an ionic strength of 0.150 M was applied (istrng=0.150). Per-residue free energy decomposition (idecomp=2) was performed to identify residues contributing to the binding interaction, with output restricted to residues within 5 Å of the receptor–ligand interface. The change in total decomposition contribution (DTDC) was used as a metric to assess residue-ligand interaction.

Results

3.1 Concentration-dependence of inhibition of I_{hERG} by nitazenes

Previous MLM work has predicted I_{hERG} inhibition by nitazenes (24). *In vitro* evaluation of five compounds presented here provides the first experimental demonstration that this is the case (Figure 1). A standard protocol was employed to elicit I_{hERG} that was comprised of an activating command from -80 mV to +20 mV followed by a repolarizing command to -40 mV (lower panels of Figures 1C and 1D; (26-28). Figure 1C shows effects of isotonitazene, while Figure 1D shows similar data for protonitazene (upper traces in Figures 1C and 1D respectively). In the example shown, 0.3 µM isotonitazene produced modest inhibition of I_{hERG} during the test pulse and of the tail current, I_{tail}, on repolarization to -40 mV. Substantially greater inhibition of I_{hERG} was seen with 1 µM isotonitazene, though more than 50% of the I_{tail} remained (Figure 1C). By contrast, in the example shown, protonitazene inhibition of I_{hERG} at each of the two concentrations (Figure 1D) was markedly greater than that seen with isotonitazene. For each drug, similar measurements were made (in separate experiments) over a range of concentrations between 0.1 and 30 µM. For each concentration tested of each drug, fractional inhibition of I_{tails} was quantified using equation 1 and pooled values at each concentration were plotted as shown in Figure 1E and fitted with equation 2. The derived half-maximal inhibitory concentration (IC_{50}) for isotonitazene was 1.32 µM, while that for protonitazene was 0.5 µM. For comparative purposes, similar measurements were made for a well-established I_{hERG} blocker, the Class Ia antiarrhythmic drug quinidine. Under the conditions of this study, quinidine exhibited an IC_{50} of 1.27 µM (Figure 1E). Summary data for IC_{50} and n_H values for all three compounds are shown in Table 1.

Experiments were extended to three other related compounds: metonitazene, etonitazene and the related piperidine benzimidazoloe brorphine. All three compounds exhibited concentration-dependent inhibition of I_{hERG}, as shown in Figure 1F and summarized in Table 1. The derived IC_{50} values lay between 0.68 µM (metonitazene) and 1.32 µM (isotonitazene). Thus, all compounds tested here inhibited I_{hERG} with IC_{50} values in the low µM or sub µM range. As highlighted in the Methods (section 2.4), isotonitazene and protonitazene were selected for more detailed investigation.

The effects of isotonitazene and protonitazene on I_{hERG} deactivation were evaluated using 1 µM concentrations with the standard +20 mV protocol. For isotonitazene, deactivation in control solution was described by fast and slow time-constants (τ_f and τ_s respectively) of 307 ± 21 ms and 2093 ± 105 ms, while in drug the values were 309 ± 25 and 2092 ± 156 ms respectively (n=8; paired t-test: P=0.94 and 0.99, respectively). The proportion of deactivation described by τ_f was unchanged (0.693 ± 0.05 and 0.625 ± 0.03 respectively). For protonitazene, τ_f and τ_s were 224 ± 17 and 1527 ± 73 ms in control, while in drug the values were 201 ± 26 and 2788 ± 181 ms (n=6; paired t-test: P=0.53 and 0.001). The proportion of deactivation described by τ_f was unchanged (0.567 ± 0.01 and 0.600 ± 0.04 respectively).

Chronic effects of isotonitazene and protonitazene exposure on hERG protein expression are shown in supplemental Figure S1. Neither drug reduced cell surface expression (CSE) of hERG channel protein. Indeed, a small (~13-16%) increase in hERG CSE was seen for both isotonitazene and protonitazene. No significant changes to total cell hERG protein expression were seen with either drug.

3.2 Voltage dependence of I_{hERG} inhibition by isotonitazene and protonitazene

The lower traces of Figure 2A and 2B show the voltage protocol used to elicit I_{hERG} at test potentials between -40 and +50 mV; drug effects on I_{tails} elicited on repolarization to -40 mV were evaluated. The upper panels of Figure 2A and 2B show representative traces for the effects of 1 µM isotonitazene. Figure 2C shows I_{tail} density-voltage plots in control and with isotonitazene. These progressively diverged with increasingly positive test commands, with significant divergence of control and drug relationships for commands to 0 mV and more positive. This is also shown in Figure 2D, which shows mean fractional block at -30 mV and +50 mV, with individual experimental values shown overlain. Fractional block was greater at +50 mV than -30 mV. Fits to the tail current data in Figure 2C with equation 3, gave activation $V_{0.5}$ values of -11.64 ± 3.61 mV in control and -13.20 ± 3.09 mV in isotonitazene (p>0.05; *k* of 6.69 ± 0.34 mV in control and 5.75 ± 0.45 in drug, p>0.05).

Figures 2E and 2F summarize the results of similar experiments with 1 µM protonitazene. This concentration of protonitazene produced a greater inhibition of hERG I_{tails} than observed for isotonitazene, consistent with the concentration-response data in Figure 1 and Table 1. For

the I_{tail} density plots (Figure 2E), inhibitory effects of protonitazene were statistically significant for commands to 0 mV and more positive (with $I_{hERG}/I_{control}$ showing a similar relationship with voltage to that for isotonitazene). Figure 2F shows mean fractional block at -30 mV and +50 mV, with individual experimental values shown overlain. Fractional block at +50 mV was significantly greater than that at -30 mV ($p<0.05$). Fits to the tail current data in Figure 2E with equation 3, gave activation $V_{0.5}$ values of -6.19 ± 5.92 mV in control and -12.76 ± 0.82 mV in protonitazene ($p<0.05$; *k* of 5.61 ± 0.45 mV in control and 4.82 ± 0.31 mV in drug, $p>0.05$). Thus, there was a modest but statistically significant leftward shift in I_{hERG} activation with protonitazene.

3.3 Time dependence of I_{hERG} inhibition by isotonitazene and protonitazene

An envelope of tails protocol (26;46) was used to evaluate development of I_{hERG} inhibition with time by the two nitazene drugs. It was comprised of progressively longer activating commands to +20 mV (between 20 and 2594 ms in duration). The protocol is shown in the lower panels on Figures 3A and 3B, while the corresponding current records are shown in the upper panels. It is evident from the experimental records shown that currents in the presence of isotonitazene diverged from those in control to a greater extent with progressively longer test pulse durations. Figure 3C shows fits to the tail current magnitudes, following normalization to maximal tail current observed during the protocol, for both control and isotonitazene conditions. These fits were used to derive time constants of activation (τ_{act}) in control and drug. It is clear that the relationship rose more quickly in the presence than in the absence of isotonitazene (with derived τ_{act} of 319.3 ± 34.29 ms in control and 144.8 ±52.51 ms in isotonitazene; $p<0.05$). Figure 3D shows similar mean data for 1 µM protonitazene, with τ_{act} of 310 ± 90.81 ms in control and 142 ±53.72 ms in protonitazene ($p<0.05$). Thus, both nitazenes produced an apparent acceleration of the time-course of I_{hERG} activation during the envelope of tails protocol. It is also notable that in the presence of either drug, after reaching a maximal value, I_{tail} amplitude decreased rather than attaining a steady-state. This is indicative of marked gating-dependence of inhibition. In order to evaluate this further, fractional inhibition of the I_{tail} was measured for each command pulse duration and was plotted as shown in Figure 3E and 3F.

Due to the apparent acceleration in I_{hERG} activation (Figures 3C and 3D), for the shortest duration voltage commands, an increase rather than inhibition in I_{hERG} was observed (resulting in an apparent negative fractional inhibition). From 228 ms onwards for isotonitazene and protonitazene positive fractional inhibition was observed and in each case this increased progressively with longer duration depolarizations. The time-course of inhibition during this protocol was obtained by quantifying the time taken for inhibition to reach half of its maximal value ($\tau_{1/2}$). For isotonitazene, the $\tau_{1/2}$ of development of inhibition was 493.4 ± 98.0 ms (n=5). For protonitazene, the $\tau_{1/2}$ of development of inhibition was 535.5 ± 124.2 ms (n=5). These observations indicate that I_{hERG} inhibition by both nitazenes was strongly gating-dependent, without any evidence for an appreciable contribution of closed-state inhibition.

3.4 Nitazene inhibition and I_{hERG} inactivation.

I_{hERG} inactivation was evaluated using the three-step protocol shown in Figure 4A, which was applied in the absence and presence of isotonitazene. An initial step to +40 mV was applied to activate and inactivate I_{hERG} followed by a "ladder" of 10 ms duration repolarising steps (from -140 mV to + 40 mV) to relieve inactivation to differing extents. Following this step a depolarization to +40 mV was applied. The magnitude of I_{hERG} during this third step depended on the extent to which the preceding 'ladder' step had relieved inactivation. Figure 4B shows representative control currents (upper panel) elicited during the third step following the 'ladder' part of the protocol (voltage shown in lower panel). Maximal current was observed following a ladder step to -140 mV, and was about half of this amplitude at ~ -30 mV. Figure 4C shows currents from the same experiment following application of isotonitazene. Under each condition the amplitude of currents following the different ladder steps was normalized to the maximal current amplitude seen during the protocol. The resulting data from 12 experiments were plotted as shown in Figure 4D and were fitted by equation 4 (Methods). From these plots inactivation $V_{0.5}$ values were obtained of -29.16 ± 2.05 in control and -29.26 ± 1.99mV in isotonitazene ($p > 0.05$; *k* of -17.16 ± 1.38 mV in control and -17.98 ±0.81 mV in drug, $p > 0.05$). Thus, there wasn't any significant voltage shift in I_{hERG} inactivation with isotonitazene, as might occur if the drug stabilized the inactivated state.

In order to probe contingency of I_{hERG} inhibition by isotonitazene on intact inactivation gating, experiments were conducted using the N588K mutation (47). An advantage of this mutation is that the N588 residue is located in the S5-Pore linker region and is remote from the pore and canonical pore binding residues. Figure 4E shows representative traces of N588K I_{hERG} in the absence and presence of 10 µM isotonitazene. Figure 4F shows the concentration response relation for N588K I_{hERG} inhibition by isotonitazene, with the WT I_{hERG} relationship shown overlain. The derived half-maximal inhibitory concentration (IC_{50}) for isotonitazene inhibition of was 6.68 µM: 5.1-fold that of WT $I_{hERG.}$ This indicates that impaired inactivation had a marked effect on isotonitazene action. Similar experiments were performed with protonitazene (Figure 4G and 4H). The derived half-maximal inhibitory concentration (IC_{50}) for protonitazene inhibition of was 1.67 µM: 3.3-fold that of WT $I_{hERG.}$ Thus, impairment of I_{hERG} inactivation had a notable, though not profound effect on the potency of both isotonitazene and protonitazene block of I_{hERG}.

3.5 Effect of pore mutants on inhibitory effects of isotonitazene and protonitazene

Aromatic residues in the S5 and S6 transmembrane segments have been implicated in the binding to hERG of a range of drugs (1;48-50). Results of experiments deploying S5 and S6 mutants are summarized in Figure 5 and Table 2. Figure 5A shows effects of the Y652A mutation on isotonitazene and protonitazene (effects of 10 µM of each drug are shown). The Y652A mutation markedly reduced drug action. Figure 5B and 5C shows concentration response relations for I_{hERG} inhibition by isotonitazene (Figure 5B) and protonitazene (Figure 5C), with IC_{50} values being 7.5-fold and 8.3-fold that for WT I_{hERG} respectively. Also shown are similar recordings from mutation of the S5 residue F557 (F557L). Again, for both isotonitazene and protonitazene inhibitory actions were reduced. Concentration-response relations for F557L are shown in Figure 5B (isotonitazene) and Figure 5C (protonitazene). For both drugs, the effects of the F557L mutation were similar to those of Y652A, with the IC_{50} for F557L I_{hERG} being 6.9-fold and 7.4-fold the WT control, respectively, for isotonitazene and protonitazene.

Further experiments were performed using the S6 F656A mutation, which typically is low expressing and requires to be measured as inward I_{hERG} in high external potassium ($[K^+]_o$ of 94 mM) (51;52). Figure 5D shows inward I_{hERG} tails for WT I_{hERG} and F656A I_{hERG}: at 10 µM both

compounds largely abolished the WT current. By contrast considerable current remained in the presence of this concentration of both isotonitazene and protonitazene for F656A. Figures 5E and 5F respectively show concentration response relations for isotonitazene and protonitazene for F656A I_{hERG}. For isotonitazene the F656A IC_{50} was 12.9-fold that of the WT control; for protonitazene the fold change was higher (73.1-fold WT control). Thus, of the residues studied F557 and Y652 appeared to be significant for hERG inhibition by both drugs and mutations of these residues had similar effects to one another for both drugs. By contrast mutation of F656 had a larger effect and was particularly notable in its effect on protonitazene.

Docking with GNINA generated nine within-pore site poses for both isotonitazene and protonitazene (Supplemental Figure S2). These poses demonstrated that the nitazene ligands could simultaneously contact the canonical aromatic pore residues F557, Y652, and F656, consistent with those identified experimentally (Figure 6). A notable difference between the two ligands was their orientation within the pore: isotonitazene adopted a more pocket-oriented conformation directed towards F557 (ca 3.69 Å), whereas protonitazene predominantly displayed pore-spanning poses. Despite this distinction, the overall pose geometries of the two ligands were broadly similar. For each nitazene, one representative pose was selected for simulation on the basis of low CNN variance (0.007 for isotonitazene, 0.02 for protonitazene) and conservation of the average pose position.

Subsequent trajectory analysis post-simulation revealed that selected poses were stable across the 5 repeats, demonstrating maximum RMSF values of 0.18 nm, shown by tertiary amide groups (Figure 7 Ai, Aii). The variable regions interestingly appeared to show similar peaks in RMSF, showing that the slight structural variation did not result in a significant change in RMSF. Moreover, repeats did not uncover a ligand rotation, proposing that these two nitazenes maintain a pore-spanning horizontal conformation, rather than a vertical insertion pose. Similarly, ligands did not demonstrate significant movement in relation to the hERG channel, as computed via RMSD (Supplemental Figure 2D).

Analysis of trajectories by gmx_MMPBSA supplemented our basis for simultaneous interactions between F557, Y652 and F656, and confirmed that binding energies between these residues were present within simulation data (Figure 7B). MMPBSA analysis was able

to show that protonitazene demonstrated an increase in DTDC to Y652 and F656, albeit that these were deemed non-significant by Mann-Whitney analysis (0.15 and 0.056 respectively p=0.05).

3.6 Effects of low $[K^+]_o$ and drug combination on nitazene actions.

Drug induced QT prolongation tends to be a multi-hit phenomenon with known risk factors including drug combination and electrolyte abnormalities, particularly hypokalemia (53). In the experiments summarized in Figure 8 we investigated the effect of reduced $[K^+]_o$ on WT I_{hERG} by isotonitazene and protonitazene. For these experiments, each drug was studied using the same standard protocol as deployed in Figure 1, but using an external solution containing 1 mM $[K^+]_o$. Effects of 0.3 µM of each drug are shown in Figure 8A (isotonitazene) and Figure 8B (protonitazene). Low $[K^+]_o$ had a marked effect on isotonitazene, as 0.3 µM of this compound produced substantial inhibition (not the case with 4 mM $[K^+]_o$). By contrast, the effect of protonitazene seemed little affected by lowering $[K^+]_o$. These observations were confirmed by constructing full concentration response relations for both compounds in low $[K^+]_o$. Figure 8C shows a marked left-ward shift of the concentration response relationship for I_{hERG} block by isotonitazene in reduced $[K^+]_o$ (IC_{50} of 0.2 µM vs 1.32 µM for 4 mM $[K^+]_o$), whereas Figure 8D shows close superimposition of the concentration response relations in reduced and normal $[K^+]_o$ for protonitazene (IC_{50} of 0.56 µM vs 0.5 µM for 4 mM $[K^+]_o$).

Nitazenes may be administered deliberately in combination with other illicitly used drugs, or as contaminants of other preparations. Therefore, in a final series of experiments, we investigated the effects of combining isotonitazene and (separately) protonitazene with fentanyl. Figure 9A shows representative traces in control and presence of 1 µM fentanyl, while Figure 9B and 9C show effects of combining each of isotonitazene (1 µM, Figure 9B) and protonitazene (0.3 µM, Figure 9C) with fentanyl. Mean I_{hERG} tail fractional block data are shown in Figure 9D and 9E. For each compound, combination with fentanyl led to significantly greater inhibition of I_{hERG} tails than was the case when either fentanyl or each nitazene was applied on their own. Thus, as might be anticipated, drug combination exacerbated I_{hERG} block by each nitazene.

4. Discussion

4.1 Nitazenes as gated state-dependent I_{hERG} inhibitors

While illicit nitazene use is recognized to be a growing threat, these drugs have no therapeutic role in clinical medicine and there is comparatively little information available on adverse effects other than respiratory depression (15) or from wider pre-clinical studies. Our recent work using *in silico* prediction methods highlighted the potential for nitazenes to interact with hERG (24). The present study is the first to provide *definitive* experimental evidence that well known nitazenes do produce I_{hERG} block. We used the antiarrhythmic drug quinidine as a positive control drug that is known to carry proarrhythmic risk (54;55); it produced an IC_{50} within the range of published values (Table 1). Isotonitazene and etonitazene were of comparable potency to quinidine as I_{hERG} inhibitors in the present study and the other drugs had lower IC_{50} values than that for quinidine.

Both the use of experimental protocols that interrogate voltage- and time- dependence of block and the use of mutations to the canonical drug binding site on hERG demonstrate that the blocking effects of protonitazene and isotonitazene (the two nitazenes that were studied in detail) arise from direct interactions of these compounds with the channel rather than as secondary effects of mu (μ) opioid receptor activation. A positive voltage-dependence of inhibition, accompanied by a modest left-ward voltage shift in activation is consistent with gated-state I_{hERG} inhibition (eg (27;46;56)). The results with the envelope of tails protocol show that protonitazene and isotonitazene produced little or no closed-state inhibition, requiring channels to undergo gating for inhibition to develop. The progressive development of blockade during applied depolarisation evident in Figure 3 is indicative of strong gating dependence of inhibition, although on its own is insufficient to distinguish between activated- and inactivated- state dependence. A number of high affinity hERG channel inhibitors show strong dependence on intact inactivation gating (e.g. (47;57-60)). For such drugs, potency of I_{hERG} inhibition can be reduced profoundly by mutations that attenuate or abolish inactivation (47;57-59). Some drugs with IC_{50} values in the μM range are strongly sensitive to inactivation attenuation: for example, the IC_{50} for ranolazine inhibition of N588K I_{hERG} was ~15-fold that of the wild-type channel (27). By contrast, other compounds – including the Class Ia antiarrhythmics quinidine and disopyramide are comparatively little affected by inactivation attenuation (47;58;59;61). Protonitazene and isotonitazene exhibited IC_{50} values for N588K

that were respectively ~ 3.3 and 5.1-fold that for WT I_{hERG}. This compares to 1.5 – 4.2 fold N588K/WT IC_{50} for disopyramide, quinidine, propafenone and amiodarone vs 11-fold for the high affinity methansulphonanilide E-4031 (47). The principal role of inactivation for conventional hERG blockers may be in facilitating optimal orientation of S6 binding residues for drug interaction (62-64). An allosteric effect is particularly likely in the case of the N588K residue, as its location in the S5-Pore linker region is remote from inner cavity binding residues.

4.2 The nitazene binding site

Although some compounds are comparatively little affected by mutations of S6 aromatic residues and the potential for non-canonical drug binding to hERG is recognized (26;46;51;65), the majority of drugs that have been examined in detail bind within the channel pore and interact with key aromatic residues (1;5;66). Y652 and F656 have long been implicated in hERG block (48;58). Cryo-EM structures of hERG indicate the presence of 4 lateral hydrophobic pockets in the tetrameric channel (67;68). In principle, such pockets may provide access to inner cavity binding sites or provide primary binding regions (26;46;66;69). F557 on S5 lies in the hydrophobic pathway and is close apposition to the side chain of Y652 (49;66;69). Within the last decade the F557L mutation has been reported to attenuate block by a number of compounds (28;46;49;69;70). Its effects on blocking potency are generally comparable to those of Y652A (28;46;49;69;70). In this study, the Y652A and F557L mutations had similar effects to one another in reducing blocking potency of both isotonitazene and protonitazene, which is consistent with prior reports on other drugs (28;46;49;69;70). However, the most striking effects in the present study arose with the F656A mutation, which increased the IC_{50} values of isotonitazene and protonitazene respectively to ~13 and ~73 fold their WT controls. This (a) implicates F656 as particularly important in nitazene inhibition of hERG and (b) is consistent with the stronger inhibitory action of protonitazene than isotonitazene. The difference in effect of F656 on the two compounds is remarkable given the close structural similarity of these nitazenes, which differ only in the specific alkyl group attached to the oxygen atom of the benzyl ring (a branched isopropoxy group in isotonitazene and a more linear propoxy group in protonitazene).

Consistent with this, our docking results support interactions between both isotonitazene and protonitazene and the aromatic residues investigated in this study (F557, Y652, and F656). Docking results further suggest that isotonitazene and protonitazene may occupy slightly different conformations within the pore, with protonitazene occupying a more central position within the pore and isotonitazene favouring more of an orientation towards the F557 pocket site. Structurally, the two compounds differ only in the alkyl group attached via the ether oxygen to the benzyl ring, a branched isopropoxy group in isotonitazene vs a more linear propoxy group in protonitazene. We observed a slightly higher RMSF value in this linear region for protonitazene, though this did not clearly contribute to the differing per-residue ΔTDC values obtained by gmx_MMPBSA. The orientation of these pore-lining residues towards the interior of the pore suggests that channel block may require simultaneous contact with multiple residues, and that a compound able to span the pore cavity may therefore have a greater capacity to cause blockade. gmx_MMPBSA analysis was unable to confidently account for the marked difference in impact of the F656A mutation-associated potency observed experimentally, as this difference in gmx_MMPBSA did not quite reach conventional statistical significance ($p=0.055$).

4.3 Clinical significance

This study establishes nitazenes as drugs that can produce acute inhibition of hERG channels. Both isotonitazene and protonitazene were evaluated for any propensity to reduce cell surface expression of hERG and neither compound reduced surface hERG levels. Thus, any hERG-related risk with these drugs is likely to result from acute inhibitory actions. Nitazenes are not used in clinical medicine and there are no recommended clinical levels of these drugs (24). In a very recent report of an isotonitazene-linked fatality, cardiac levels of 20 ng/g were reported (roughly equivalent to 50 nM) (71). While such an isotonitazene level would produce comparatively low levels of I_{hERG} inhibition with normal $[K^+]_o$, in principle it could give a substantial inhibition under conditions of hypokalemia (blood $[K^+]$ was not given in (71)). Current data in the UK National Programme on Substance Use Mortality (NPSUM) show cardiovascular involvement in a number of nitazene-related deaths, but are insufficient to implicate direct cardiac electrophysiological effects (Copeland *et al*, personal observations).

On the other hand, in a fatality linked to protonitazene overdose, the [protonitazene] in cardiac blood was 1400 ng/ml (equivalent to 3.41 µM) (72). While post-mortem concentrations should be extrapolated to *in vivo* or experimental concentrations with caution, it is notable that our data indicate that at such a concentration substantial I_{hERG} block would be observed. Most cases of drug-induced QT interval prolongation are associated with the additional presence of one or more risk factors (53). The actions of quinidine and dofetilide have long been known to be sensitive to external $[K^+]$ (73). Our data on isotonitazene demonstrate that the drug's action was considerably more potent in the context of simulated hypokalemia, while for protonitazene this was not the case. Extracellular $[K^+]$ can modulate I_{hERG} inactivation (2;32). It was notable that high $[K^+]_o$ did not markedly affect IC_{50} of either drug, but that low $[K^+]_o$ did so for isotonitazene. It is notable that the N588K mutation had a greater effect on isotonitazene than on protonitazene. It is possible, therefore, that for isotonitazene (but not protonitazene) S6 positioning during inactivation gating at reduced $[K^+]_o$ was more favourable for isotonitazene interaction with key binding residues.

Many nitazene users either take nitazenes alongside other drugs or, (unknowingly) consume preparations in which nitazenes are mixed with other illicitly used drugs; thus nitazenes can be taken at the same time as with benzodiazepines, fentanyl, heroin and cocaine (15;16;19;72). Concomitant administration of >1 QT prolonging drug is a known risk in drug-induced QT syndrome (53). Both cocaine and fentanyl are known hERG channel inhibitors (74-76) and ingestion of nitazenes together with these drugs might therefore compound risk. Indeed, our experimental results demonstrate that combining fentanyl with either protonitazene or isotonitazene produced greater I_{hERG} inhibition than either nitazene or fentanyl on its own. This highlights that nitazene users should be advised that both deliberate and inadvertent combination of nitazenes with fentanyl is likely to increase the potential for cardiac electrophysiological effects, quite aside from compounding risk of respiratory depression. Moreover, it would probably be prudent to avoid combining nitazenes with any known hERG blocking/QT prolonging drug and this is a consideration for clinicians treating individuals known to use nitazenes. Additionally, and consistent with our findings on brorphine, a recent preprint ((83), a publication pre-peer review) provides independent evidence that "orphine" opioids can inhibit hERG. Thus, clinicians should also be mindful of

the potential for hERG blockade when treating individuals known to use brorphine or other orphine opioids.

Limitations and conclusions

This study has investigated the propensity of nitazene drugs to inhibit hERG potassium channels and the underlying mechanisms by which inhibition occurs. If nitazenes also produce inhibition of other cardiac ion channels at overlapping concentrations, this could exacerbate or offset hERG/I_{Kr} inhibition and thereby influence overall effects on ventricular repolarisation (77). Therefore, future studies should investigate effects of nitazene drugs against a wider range of cardiac ion channel targets than hERG alone. Although it is important that this limitation is noted, it does not detract from the facts that this study is: (i) the first direct demonstration of hERG channel block by any nitazene and (ii) a demonstration that multiple nitazenes can inhibit I_{hERG} at micromolar and submicromolar concentration and (iii) to our knowledge, one of the first studies to demonstrate direct inhibition of any ion channel by this class of drug.

Acknowledgements

The authors thank Professor Will Fuller (University of Glasgow) for help with FRT/TO plasmids, Professor Eamonn Kelly (University of Bristol) for assistance with fentanyl and nitazenes and Professor Graeme Henderson (University of Bristol) for valuable discussion.

Funding

This work was funded by the British Heart Foundation (FS/PhD/24/29563, FS/PhD/25/29771, FS/19/44/34424, PG/23/11356, PG/24/11849). An equipment grant from the Medical Research Council is also gratefully acknowledged (MR/X012670/1).

Author contributions. JCH conceived the study. JCH, SCH, RC, MRC designed the study. JCH, SCH, RC obtained funding and provided supervision. AEH also provided supervision. Material

preparation, data collection and analysis were performed by MRC, MB, TO, OH, YZ, HC. The first draft of the manuscript was produced by JCH, MRC, SCH, TO, RC, YZ. All authors reviewed/commented on manuscript drafts prior to submission. All authors read and approved the final manuscript.

Availability of data and materials.

The data for the study are included in the manuscript and supplementary information. Materials for the study will be made available on reasonable request.

Code availability.

Docking was performed against the Dickson pore model of hERG (37). Docked poses are available from RC on request.

Declarations

Ethics approval and consent to participate: N/A.

Consent for publication: N/A.

Competing interests: The authors declare that they have no actual or potential competing interests.

Compound	IC_{50} (µM) [95% C.I.]	n_H [95% C.I.]	Number of Cells	Published IC_{50} range	Example References
Isotonitazene	1.32 [1.16-1.51]	1.38 [1.16-1.67]	7-12	N/A	
Protonitazene	0.50 [0.41–0.62]	1.16 [0.93–1.47]	6	N/A	
Metonitazene	0.68 [0.52–0.90]	0.98 [0.77–1.27]	8	N/A	
Etonitazene	1.28 [1.16–1.41]	1.30 [1.16-1.47]	9	N/A	
Brorphine	0.93 [0.77- 1.13]	1.15 [0.95-1.42]	5-6	N/A	
Quinidine	1.27 [1.06–1.51]	1.02 [0.87-1.22]	5	0.3-8.6	(78-82)

Table 1 Concentration response summary data for nitazene opioids

Summary data derived from fits to concentration response relations shown in Figure 1, using equation 2 (Methods). For both IC_{50} and n_H values means and 95% confidence intervals (C.I.) are shown. 'n' values refer to number of replicates used for concentration-response data. Quinidine was used as a known reference compound, with the observed IC_{50} value from this study lying within the range of published IC_{50} values.

Drug	Construct	n	IC_{50} (μM)	95% C.I. (μM)	n_H	95% C.I.	Fold of WT IC_{50}
Isotonitazene	WT	7-12	1.32	1.16-1.51	1.38	1.16-1.67	1
Isotonitazene	Y652A	6	9.89	7.24-13.91	0.72	0.54-0.99	7.5
Isotonitazene	F557L	5	9.11	5.94-13.79	0.68	0.52-0.91	6.9
Protonitazene	WT	6	0.5	0.41-0.62	1.16	0.93-1.47	1
Protonitazene	Y652A	7	4.17	3.33-5.21	0.85	0.71-1.03	8.3
Protonitazene	F557L	5-6	3.69	2.97-4.60	0.97	0.8-1.19	7.4
Isotonitazene	WT inward	5	1.02	0.97-1.15	1.09	0.97-1.24	1
Isotonitazene	F656A	5-9	13.18	8.42-21.21	0.44	0.35-0.55	12.9
Protonitazene	WT inward	6	0.44	0.37-0.54	0.94	0.79-1.14	1
Protonitazene	F656A	5	32.15	14.62-87.71	0.34	0.22-0.47	73.1

Table 2 Concentration-response summary data for nitazene inhibition of WT and mutant hERG channels

Summary data were derived from fits to concentration-response relationships shown in Figure 5, using equation 2 (Methods). For both IC_{50} and n_H values, 95% confidence intervals (C.I.) are shown with 'n' values referring to the number of replicates used for concentration-response data. Fold-shift values were calculated relative to the matched WT condition.

Figure Legends

Figure 1. hERG inhibition by nitazenes. (**A, B**) Chemical structures of isotonitazene (**A**) and protonitazene (**B**). (**C,D**) I_{hERG} current traces (upper) recorded using a standard +20 mV command protocol (lower) under control conditions and in the presence of isotonitazene (**C**) and protonitazene (**D**). Two concentrations (0.3 and 1 µM) are shown to illustrate concentration-dependent inhibition. (**E**) Six concentrations of protonitazene, isotonitazene, and quinidine (used as a reference compound), ranging from 100 nM to 30 µM, were tested to generate a concentration-response plot (fitted with equation 2 methods) (n=5-12). (**F**) Concentration–response relationships for etonitazene, metonitazene, and brorphine, plotted and fitted as in (**E**) (n=5-9).

Figure 2. Voltage dependence of I_{hERG} inhibition by isotonitazene and protonitazene. (**A, B**) Representative I_{hERG} traces (upper) recorded using a current-voltage (I–V) protocol (lower) under control conditions (**A**) and 1 µM isotonitazene (**B**). (**C**) Mean tail current density–voltage relationships for I_{hERG} in control and in the presence of 1 µM isotonitazene. Tail current density was measured on repolarisation to -40 mV following test pulses between -40 and +50 mV fitted with equation 3 gave $V_{0.5}$ values of -11.64 ± 3.61 mV in control and -13.20 ± 3.09 mV in isotonitazene, with *k* values of 6.69 ± 0.34 mV and 5.75 ± 0.45 mV, respectively (n=8). (**D**) Fractional block of I_{hERG} by isotonitazene at -30 mV and +50 mV compared (n=7). (**E**) Mean tail current density–voltage relationships for I_{hERG} in control and in the presence of 1 µM protonitazene, plotted and analysed as in (**C**). Fits to the tail current data gave $V_{0.5}$ values of -6.19 ± 5.92 mV in control and -12.76 ± 0.82 mV in protonitazene, with *k* values of 5.61 ± 0.45 mV and 4.82 ± 0.31 mV, respectively (n=6). (**F**) Fractional block of I_{hERG} by protonitazene at -30 mV and +50 mV, compared as in (**D**) (n=7). Statistical comparisons were made using repeated-measures two-way ANOVA with post hoc comparisons for current density–voltage relationships and paired t-tests for fractional block comparisons. *P < 0.05; **P < 0.01; ***P < 0.001; ****P < 0.0001.

Figure 3. Time-dependence of I_{hERG} inhibition by isotonitazene and protonitazene.

(**A, B**) Representative I_{hERG} currents recorded using the envelope-of-tails protocol under control conditions (**A**) and following application of 1 µM isotonitazene (**B**). The corresponding voltage command protocol is shown below. Cells were depolarised to +20 mV for progressively increasing pulse durations before repolarisation to -40 mV, at which peak tail current amplitude was measured. (**C**) Normalised tail current amplitudes plotted against pulse duration under control conditions and in the presence of 1 µM isotonitazene. Tail current amplitudes were normalised to the maximal tail current observed and fitted with a one-phase association function to give the τ values shown in the "Results" text (n=5). (**D**) Normalised tail current amplitudes plotted against pulse duration under control conditions and in the presence of 1 µM protonitazene, analysed as in (**C)** (n=5). (**Ei, Fi**) Fractional block of I_{hERG} plotted against depolarising pulse duration for 1 µM isotonitazene (n=5) (**Ei**) and 1 µM protonitazene (n=5) (**Fi**). Fractional block values were fitted with a bi-exponential association

function to describe the time-course of development of inhibition. (**Eii, Fii)** Expanded view of the early pulse durations from the fractional block plots shown in Ei and Fi (n=5).

Figure 4. Effects of isotonitazene on I_{hERG} inactivation. (**A**) Voltage protocol used to assess the voltage dependence of I_{hERG} inactivation. I_{hERG} was first activated and inactivated by a depolarising step to +40 mV, followed by 10 ms repolarising steps from -140 mV to +40 mV in 20 mV increments, to relieve inactivation. The membrane potential was then stepped back to +40 mV to elicit transient currents. The inset shows the "ladder portion" of the protocol. (**B, C**) Representative I_{hERG} current traces under control conditions (**B**) and following application of 1 µM isotonitazene (**C**). The corresponding voltages are shown beneath the current traces. (**D**) Normalised inactivation relationships for control and 1 µM isotonitazene. Current amplitudes were normalised to the maximal current recorded during the protocol and fitted with a Boltzmann function. $V_{0.5}$ values were -29.16 ± 2.05 mV in control and -29.26 ± 1.99 mV in 1 µM isotonitazene; *k* values were -17.16 ± 1.38 mV and -17.98 ± 0.81 mV, respectively (n=12; p>0.05). (**E**) Representative N588K I_{hERG} traces recorded under control conditions (black) and 10 µM isotonitazene (green). (**F**) Concentration-response relationship for isotonitazene inhibition of N588K I_{hERG} and WT I_{hERG} (n=5). (**G**) Representative N588K I_{hERG} traces recorded under control conditions (black) and 10 µM protonitazene (green). (**H**) Concentration-response relationship for protonitazene inhibition of N588K I_{hERG} and WT I_{hERG} (n=6). Concentration-response relationships were fitted with the Hill equation with data shown as mean ± SEM.

Figure 5. Block of I_{hERG} for wild-type and mutant channels. (**A**) Representative current traces showing the effects of 10 µM isotonitazene and 10 µM protonitazene on WT, Y652A and F557L hERG channels. Traces were recorded using the standard voltage protocol as shown in the panel. (**B, C**) Concentration-response relationships for inhibition of WT (n=7-12), Y652A (n=6) and F557L (n=5) I_{hERG} by isotonitazene (**B**) and inhibition of WT (n=6), Y652A (n=7) and F557L (n=5-6) I_{hERG} by protonitazene (**C**). Fractional block was calculated and data were fitted with the Hill equation. WT relationships are shown superimposed for comparison with mutant channel responses. (**D**) Representative inward current traces recorded from WT and F656A under control conditions and in the presence of 10 µM isotonitazene or 10 µM protonitazene. (**E, F**) Concentration-response relationships for inhibition of WT and F656A by isotonitazene (**E**) (n=5-9) and protonitazene (**F**) (n=5-6) analysed as in (**B, C**).

Figure 6. Molecular docking of isotonitazene and protonitazene

(A) and **(B)** respectively show selected poses for isotonitazene (top, cyan) and protonitazene (bottom, purple). Both drugs show poses that simultaneously contact the three aromatic proposed pore residues F557 (green), Y652 (yellow) and F656 (red). Noticeably, protonitazene occupies a more central orientation within the pore; however, both drugs show a flat horizontal orientation rather than a vertical insertion into the pore. Distances to proximal residues of interest are included in Angstroms.

Figure 7. Further in silico analysis of isotonitazene and protonitazene binding interactions

(A) show RMSF by B-Factor and mean per atom RMSF of isotonitazene and protonitazene during MD simulation. The RMSF (nm) of ligand heavy atoms is shown across five independent simulation repeats, for **(Ai)** isotonitazene and **(Aii)** protonitazene. Atoms are grouped and labelled according to their constituent functional group: amide (AMI), benzyl (BZ), variable region (VR), benzimidazole (BZIM), and nitro (NIT).

(B) Summed residue enthalpy by ΔTDC across interacting chain. Total per-residue ΔTDC, kcal/mol was summed across each ligand-interacting chain. Per-residue values were summed within each chain, then averaged across 5 independent replicate simulations. Error bars represent SEM.

Figure 8. Effect of reduced extracellular K^+ on nitazene inhibition of I_{hERG}.

(**A, B**) Representative I_{hERG} traces recorded using standard voltage protocol under low extracellular K^+ conditions, showing the effects of 0.3 µM isotonitazene (**A**) and 0.3 µM protonitazene (**B**). The corresponding voltage protocol is shown below each set of current traces. Currents were elicited by depolarisation to +20 mV followed by repolarisation to -40 mV, at which peak tail current amplitude was measured. (**C**) Concentration-response relationship for isotonitazene inhibition of I_{hERG} recorded in standard 4 mM extracellular K^+ (solid black line) inhibited I_{hERG} with an IC_{50} of 1.32 µM and n_H 1.38 (n=7-12) and reduced 1 mM extracellular K^+ inhibited I_{hERG} with an IC_{50} of 0.2 µM with n_H 1.19 (dashed black line) (n=5). (**D**) Concentration-response relationship for protonitazene inhibition of I_{hERG} recorded in 4 mM inhibited I_{hERG} with an IC_{50} of 0.5 µM and n_H 1.16 (n=6) and 1 mM extracellular K^+ inhibited I_{hERG} with an IC_{50} of 0.56 µM with n_H 1.08 (n=6).

Figure 9. Effects of drug combinations on the inhibition of I_{hERG}.

(**A–C**) Representative I_{hERG} traces recorded using the standard +20 mV protocol under control conditions and following application of 1 µM fentanyl alone (**A**), a combined mixture of 1 µM

isotonitazene and 1 µM fentanyl (**B**), or a combined mixture of 0.3 µM protonitazene and 1 µM fentanyl (**C**). Tail current amplitude was measured on repolarisation to -40 mV. (**D**) Summary of percentage I_{hERG} block produced by 1 µM fentanyl, 1 µM isotonitazene and 1 µM isotonitazene + 1 µM fentanyl combination. (**E**) Summary of the percentage I_{hERG} block produced by 1 µM fentanyl, 0.3 µM protonitazene, and 0.3 µM protonitazene + 1 µM fentanyl combination. Block was calculated from peak tail current amplitudes as $1 - I_{drug}/I_{control}$ and expressed as percentage block. Statistical comparisons were made using ordinary one-way ANOVA with Tukey's multiple comparisons test. *P < 0.05; **P < 0.01; ***P < 0.001; ****P < 0.0001.

References

(1) Sanguinetti MC, Tristani-Firouzi M (2006) hERG potassium channels and cardiac arrhythmia. Nature 440(7083):463-469.

(2) Sanguinetti MC, Jiang C, Curran ME, Keating MT (1995) A mechanistic link between an inherited and an acquired cardiac arrhythmia: HERG encodes the I_{Kr} potassium channel. Cell 81:299-307.

(3) Trudeau MC, Warmke JW, Ganetzky B, Robertson GA (1995) HERG, an inward rectifier in the voltage-gated potassium channel family. Science 269: 92-95.

(4) Hancox JC, DU CY, Butler A, Zhang Y, Dempsey CE, Harmer SC, et al. (2023) Pro-arrhythmic effects of gain-of-function potassium channel mutations in the short QT syndrome. Philos Trans R Soc Lond B Biol Sci 378(1879):20220165.

(5) Hancox JC, McPate MJ, El Harchi A, Zhang YH (2008) The hERG potassium channel and hERG screening for drug-induced torsades de pointes. Pharmacology and Therapeutics 2008;119:118-132.

(6) Ritchie D, Forget P (2026) Pain Medicine and the Opioid Crisis: Time to Own Our Responsibility! Eur J Pain 30(4):e70263.

(7) Canning P, Carnevale DM, Kostyun R, Kamin R (2025) Opioid Epidemic Through the Lens of Prehospital Emergency Care: A 5-Year Descriptive Analysis of the Statewide Opioid Response Directive (SWORD) Surveillance Program. Prehosp Emerg Care Sep 30;1-6.

(8) Buckley RJ, Yang D, D'Onofrio G, Perman SM (2026) Overdose-Related Cardiac Arrest in the Era of the Opioid Epidemic. Crit Care Clin 2026 42(1):215-233.

(9) Behzadi M, Joukar S, Beik A (2018) Opioids and Cardiac Arrhythmia: A Literature Review. Med Princ Pract 27(5):401-414.

(10) Golibkhon A, kbar Gafur UB, Makhamadjonov Farkhod UM (2023) Opioid Agents and Cardiac Arrhythmia: A Literature Review. Cureus 15(4):e38007.

(11) Katchman AN, McGroary KA, Kilborn MJ, Kornick CA, Manfredi PL, Woosley RL, et al (2002). Influence of opioid agonists on cardiac human ether-a-go-go-related gene K^+ currents. J Pharmacol Exp Ther 303(2):688-694.

(12) Zunkler BJ, Wos-Maganga M (2010) Comparison of the effects of methadone and heroin on human ether-a-go-go-related gene channels. Cardiovasc Toxicol 10(3):161-165.

(13) Fanoe S, Jensen GB, Sjogren P, Korsgaard MP, Grunnet M (2009) Oxycodone is associated with dose-dependent QTc prolongation in patients and low-affinity inhibiting of hERG activity in vitro. Br J Clin Pharmacol 67(2):172-179.

(14) Ujvary I, Christie R, Evans-Brown M, Gallegos A, Jorge R, de MJ, et al (2021) DARK Classics in Chemical Neuroscience: Etonitazene and Related Benzimidazoles. ACS Chem Neurosci 12(7):1072-1092.

(15) Pergolizzi J, Jr., Raffa R, LeQuang JAK, Breve F, Varrassi G (2023) Old Drugs and New Challenges: A Narrative Review of Nitazenes. Cureus 15(6):e40736.

(16) Montanari E, Madeo G, Pichini S, Busardo FP, Carlier J (2022) Acute Intoxications and Fatalities Associated With Benzimidazole Opioid (Nitazene Analog) Use: A Systematic Review. Ther Drug Monit 44(4):494-510.

(17) Bade R, Eaglesham G, Shimko KM, Mueller J (2023) Quantification of new psychoactive substances in Australian wastewater utilising direct injection liquid chromatography coupled to tandem mass spectrometry. Talanta 251:123767.

(18) Bade R, Nadarajan D, Driver EM, Halden RU, Gerber C, Krotulski A, et al. (2024) Wastewater-based monitoring of the nitazene analogues: First detection of protonitazene in wastewater. Sci Total Environ;920:170781.

(19) Pereira JRP, Quintas A, Neng NR (2025) Nitazenes: The Emergence of a Potent Synthetic Opioid Threat. Molecules;30(19).

(20) Holland A, Copeland CS, Shorter GW, Connolly DJ, Wiseman A, Mooney J, et al (2024) Nitazenes-heralding a second wave for the UK drug-related death crisis? Lancet Public Health 9(2):e71-e72.

(21) Chen S, Aldabergenov D, Alotaibi KS, Holland A, Moore R, Wood R, et al (2026) Is nitazene-related mortality underestimated? Findings from an in vivo and ex vivo rat study and pharmacoepidemiological analysis of coroner-reported deaths. Clin Toxicol (Phila) 64(4):311-323.

(22) Amaducci A, Aldy K, Campleman SL, Li S, Meyn A, Abston S, et al (2023) Naloxone Use in Novel Potent Opioid and Fentanyl Overdoses in Emergency Department Patients. JAMA Netw Open 6(8):e2331264.

(23) Kurach L, Chlopas-Konowalek A, Budzynska B, Zawadzki M, Szpot P, Boguszewska-Czubara A (2021) Etazene induces developmental toxicity in vivo Danio rerio and in silico studies of new synthetic opioid derivative. Sci Rep 11(1):24269.

(24) Hancox JC, Wang Y, Copeland CS, Zhang H, Harmer SC, Henderson G (2024) Nitazene opioids and the heart: Identification of a cardiac ion channel target for illicit nitazene opioids. J Mol Cell Cardiol Plus 10:100118.

(25) Zhou Z, Gong Q, Ye B, Fan Z, Makielski JC, Robertson GA, et al (1998) Properties of HERG channels stably expressed in HEK 293 cells studied at physiological temperature. Biophys J 74:230-241.

(26) Al-Moubarak E, Shiels El Harchi A, Zhang Y, Du C, Hanington O, Harmer SC, et al (2021) Inhibition of the hERG potassium channel by phenanthrene: a polycyclic aromatic hydrocarbon pollutant. Cell Mol Life Sci 78(23):7899-7914.

(27) Du C, Zhang Y, El Harchi A, Dempsey CE, Hancox JC (2014) Ranolazine inhibition of hERG potassium channels: Drug-pore interactions and reduced potency against inactivation mutants. J Mol Cell Cardiol 74C:220-230.

(28) Helliwell MV, Zhang Y, El Harchi A, Du C, Hancox JC, Dempsey CE (2018) Structural implications of hERG K(+) channel block by a high affinity minimally-structured blocker. J Biol Chem 293: 7040-7057.

(29) Zhang Y, Colenso CK, El Harchi A, Cheng H, Witchel HJ, Dempsey CE, et al (2016). Interactions between amiodarone and the hERG potassium channel pore determined with mutagenesis and in silico docking. Biochem Pharmacol;113:24-35.

(30) Zhang Y, Grimwood AL, Hancox JC, Harmer SC, Dempsey CE (2022) Evolutionary coupling analysis guides identification of mistrafficking-sensitive variants in cardiac K(+) channels: Validation with hERG. Front Pharmacol;13:1010119.

(31) Congreve SD, Main A, Butler AS, Gao X, Brown E, Du C, et al (2023) Palmitoylation regulates the magnitude of HCN4-mediated currents in mammalian cells. Front Physiol;14:1163339.

(32) Melgari D, Du C, El Harchi A, Zhang Y, Hancox JC (2014). Suppression of the hERG potassium channel response to premature stimulation by reduction in extracellular potassium concentration. Physiol Rep; 2(10) e12165

(33) Al Moubarak E, Zhang Y, Dempsey CE, Zhang H, Harmer SC, Hancox JC (2020). Serine mutation of a conserved threonine in the hERG K+ channel S6-pore region leads to loss-of-function through trafficking impairment. Biochem.Biophys Res.Commun. 526, 1085-1091.

(34) McPate MJ, Duncan RS, Milnes JT, Witchel HJ, Hancox JC (2005) The N588K-HERG K^+ channel mutation in the 'short QT syndrome': mechanism of gain-in-function determined at 37 ^oC. Biochem Biophys Res Comm; 334: 441-449.

(35) McNutt AT, Francoeur P, Aggarwal R, Masuda T, Meli R, Ragoza M, et al (2021) GNINA 1.0: molecular docking with deep learning. J Cheminform 9;13(1):43.

(36) Eberhardt J, Santos-Martins D, Tillack AF, Forli S (2021) AutoDock Vina 1.2.0: New Docking Methods, Expanded Force Field, and Python Bindings. J Chem Inf Model ;61(8):3891-3898.

(37) Dickson CJ, Velez-Vega C, Duca JS (2020). Revealing Molecular Determinants of hERG Blocker and Activator Binding. J Chem Inf Model 60(1):192-203.

(38) Kim S, Lee J, Jo S, Brooks CL, III, Lee HS, Im W (2017) CHARMM-GUI ligand reader and modeler for CHARMM force field generation of small molecules. J Comput Chem;38(21):1879-1886.

(39) Wu EL, Cheng X, Jo S, Rui H, Song KC, vila-Contreras EM, et al (2014) CHARMM-GUI Membrane Builder toward realistic biological membrane simulations. J Comput Chem 35(27):1997-2004.

(40) Lee J, Patel DS, Stahle J, Park SJ, Kern NR, Kim S, et al (2019) CHARMM-GUI Membrane Builder for Complex Biological Membrane Simulations with Glycolipids and Lipoglycans. J Chem Theory Comput 15(1):775-786.

(41) Sondergaard CR, Olsson MH, Rostkowski M, Jensen JH (2011) Improved Treatment of Ligands and Coupling Effects in Empirical Calculation and Rationalization of pKa Values. J Chem Theory Comput;7(7):2284-2295.

(42) Van der Spoel D, Lindahl E, Hess B, Groenhof G, Mark AE, Berendsen HJ (2005) GROMACS: fast, flexible, and free. J Comput Chem;26(16):1701-1718.

(43) Abraham MJ, Murtola T, Schulz R, Pall S, Smith JC, Hess B, et al (2015) GROMACS: High performance molecular simulations through multi-level parallelism from laptops to supercomputers. SoftwareX 1-2, 19-25. 1-9-2015.

(44) Valdes-Tresanco MS, Valdes-Tresanco ME, Valiente PA, Moreno E (2021) gmx_MMPBSA: A New Tool to Perform End-State Free Energy Calculations with GROMACS. J Chem Theory Comput 17(10):6281-6291.

(45) Greene D, Qi R, Nguyen R, Qiu T, Luo R (2019) Heterogeneous Dielectric Implicit Membrane Model for the Calculation of MMPBSA Binding Free Energies. J Chem Inf Model; 59(6):3041-3056.

(46) Cheng H, Upex C, Du C, Copeland C, Henderson G, Harmer SC, et al (2025) Noncanonical pharmacological inhibition of the hERG K^+ channel by a synthetic cannabinoid. Biochem Pharmacol 242(Pt 1):117257.

(47) McPate MJ, Duncan RS, Hancox JC, Witchel HJ (2008). Pharmacology of the short QT syndrome N588K-hERG K+ channel mutation: differential impact on selected class I and class III antiarrhythmic drugs. Br J Pharmacol 155:957-966.

(48) Mitcheson JS, Chen J, Lin M, Culberson C, Sanguinetti MC (2000) A structural basis for drug-induced long QT syndrome. Proc Natl Acad Sci U S A 97:12329-12333.

(49) Saxena P, Zangerl-Plessl EM, Linder T, Windisch A, Hohaus A, Timin E, et al (2016) New potential binding determinant for hERG channel inhibitors. Sci Rep;6:24182.

(50) Butler A, Helliwell MV, Zhang Y, Hancox JC, Dempsey CE (2019) An Update on the Structure of hERG. Front Pharmacol;10:1572.

(51) Milnes JT, Crociani O, Arcangeli A, Hancox JC, Witchel HJ (2003) Blockade of HERG potassium currents by fluvoxamine: incomplete attenuation by S6 mutations at F656 or Y652. Br J Pharmacol 139(5):887-898.

(52) Melgari D, Brack KE, Zhang C, Zhang Y, El Harchi A, Mitcheson JS, et al (2015) hERG potassium channel blockade by the HCN channel inhibitor bradycardic agent ivabradine. J Am Heart Assoc 2015;4(4) e001813.

(53) Zeltser D, Justo D, Halkin A, Prokhorov V, Heller K, Viskin S (2003) Torsade de pointes due to noncardiac drugs: most patients have easily identifiable risk factors. Medicine (Baltimore);82(4):282-90.

(54) Yap YG, Camm AJ (2003) Drug induced QT prolongation and torsades de pointes. HEART;(89):1363-1372.

(55) Redfern WS, Carlsson L, Davis AS, Lynch WG, MacKenzie I, Palethorpe S, et al.(2003) Relationships between preclinical cardiac electrophysiology, clinical QT interval prolongation and torsade de pointes for a broad range of drugs: evidence for a provisional safety margin in drug development. Cardiovas Res;58:32-45.

(56) Hancox JC, Melgari D, Dempsey CE, Brack KE, Mitcheson J, Ng GA (2015). hERG potassium channel inhibition by ivabradine may contribute to QT prolongation and risk of torsades de pointes. Ther Adv Drug Saf;6(4):177-179.

(57) Ficker E, Jarolimek W, Kiehn J, Baumann A, Brown AM (1998) Molecular determinants of dofetilide block of HERG K channels. Circ Res;82:386-395.

(58) Lees-Miller JP, Duan Y, Teng GQ, Duff HJ (2000) Molecular determinant of high affinity dofetilide binding to HERG1 expressed in Xenopus oocytes: involvement of S6 sites. Molecular Pharmacology 57:367-74.

(59) Perrin MJ, Kuchel PW, Campbell TJ, Vandenberg JI (2008) Drug binding to the inactivated state is necessary but not sufficient for high-affinity binding to human ether-à-go-go-related gene channels. Mol Pharmacol 74:1443-52.

(60) Ngo K, Yang PC, Yarov-Yarovoy V, Clancy CE, Vorobyov I (2025) Harnessing AlphaFold to reveal hERG channel conformational state secrets. Elife Jul 14;13.RP104901

(61) McPate MJ, Duncan RS, Witchel HJ, Hancox JC (2006) Disopyramide is an effective inhibitor of mutant HERG K^+ channels involved in variant 1 short QT syndrome. J Mol Cell Cardiol 41:563-536.

(62) Chen J, Seebohm G, Sanguinetti MC (2002) Position of aromatic residues in the S6 domain, not inactivation, dictates cisapride sensitivity of HERG and eag potassium channels. Proc Natl Acad Sci USA 99:12329-12333.

(63) Wu W, Gardner A, Sanguinetti MC (2015) The Link between Inactivation and High-Affinity Block of hERG1 Channels. Mol Pharmacol 87(6):1042-1050.

(64) Zhang Y, El Harchi A, James AF, Oiki S, Dempsey CE, Hancox JC (2024). Stereoselective block of the hERG potassium channel by the Class Ia antiarrhythmic drug disopyramide. Cell Mol Life Sci;81(1):466.

(65) Zunkler BJ (2024). Multiple hERG channel blocking pathways: implications for macromolecules. Trends Pharmacol Sci;45(8):671-677.

(66) Butler A, Helliwell MV, Zhang Y, Hancox JC, Dempsey CE (2019) An Update on the Structure of hERG. Front Pharmacol;10:1572.

(67) Wang W, MacKinnon R (2017) Cryo-EM Structure of the Open Human Ether-a-go-go-Related K+ Channel hERG. Cell 169(3):422-430.

(68) Asai T, Adachi N, Moriya T, Oki H, Maru T, Kawasaki M, et al (2021) Cryo-EM Structure of K(+)-Bound hERG Channel Complexed with the Blocker Astemizole. Structure 29(3):203-212.

(69) Perissinotti L, Guo J, Kudaibergenova M, Lees-Miller J, Ol'khovich M, Sharapova A, et al (2019). The Pore-Lipid Interface: Role of Amino-Acid Determinants of Lipophilic Access by Ivabradine to the hERG1 Pore Domain. Mol Pharmacol 96(2):259-271.

(70) Cheng H, Du C, Zhang Y, James AF, Dempsey CE, Abdala AP, et al (2019) Potent hERG channel inhibition by sarizotan, an investigative treatment for Rett Syndrome. J Mol Cell Cardiol;135:22-30.

(71) J.-J. Bendjilali-Sabiani JJ, Eiden C, Lossois M, Martrille L, Peyriere H, Mathieu O (2026) Postmortem distribution of isotonitazene and its three metabolites in the first lethal case observed in France. Forensic Sci Int;379:112763.

(72) Edinoff AN, Martinez GD, Vining SP, Vasterling ME, Jackson ED, Murnane KS, et al.(2023) New Synthetic Opioids: Clinical Considerations and Dangers. Pain Ther 12(2):399-421.

(73) Yang T, Roden DM (1996) Extracellular potassium modulation of drug block of Ikr. Implications for torsade de pointes and reverse use-dependence. Circulation; 93(3):407-411.

(74) Tschirhart JN, Li W, Guo J, Zhang S (2019) Blockade of the Human Ether A-Go-Go-Related Gene (hERG) Potassium Channel by Fentanyl. Mol Pharmacol 95(4):386-397.

(75) O'Leary ME (2001) Inhibition of human ether-a-go-go potassium channels by cocaine. Mol Pharmacol 59(2):269-277.

(76) Zhang S, Rajamani S, Chen Y, Gong Q, Rong Y, Zhou Z, et al (2001). Cocaine blocks HERG, but not KvLQT1+minK, potassium channels. Mol Pharmacol 59(5):1069-1076.

(77) Fermini B, Hancox JC, bi-Gerges N, Bridgland-Taylor M, Chaudhary KW, Colatsky T, et al (2016) A New Perspective in the Field of Cardiac Safety Testing through the Comprehensive In Vitro Proarrhythmia Assay Paradigm. J Biomol Screen 21(1):1-11.

(78) Ishii K, Kondo K, Takahashi M, Kimura M, Endoh M (2001) An amino acid residue whose change by mutation affects drug binding to the HERG channel. FEBS Lett;506:191-195.

(79) Paul AA, Witchel HJ, Hancox JC (2002) Inhibition of heterolgously expressed HERG potassium channels by flecainide and comparison with quinidine, propafenone and lignocaine. Br J Pharmacol;136:717-729.

(80) Ducroq J, Printemps R, Guilbot S, Gardette J, Salvetat C, Le GM (2007) Action potential experiments complete hERG assay and QT-interval measurements in cardiac preclinical studies. J Pharmacol Toxicol Methods;56(2):159-170.

(81) McBride BF, Yang T, Liu K, Urban TJ, Giacomini KM, Kim RB, et al (2009) The organic cation transporter, OCTN1, expressed in the human heart, potentiates antagonism of the HERG potassium channel. J Cardiovasc Pharmacol 54(1):63-71.

(82) Weerapura M, Nattel S, Chartier D, Caballero R, Hebert TF (2002) A comparison of currents carried by HERG with and without the coexpression of MiRP1, and the native rapid delayed rectifier current. Is MiRP1 the missing link? J Physiol 540:15-27.

(83) Norman C, Ottoson NE, Holmberg JR, Norlund M, Hormon EJ, Wilkstrom M, Kronstrand R, Persson M, Green H (2026). *In vitro* activation of μ opioid receptor and cardiac voltage gated potassium channels hERG and Kv7.1/KCNE1 of orphine analogs and their detections in forensic casework. Research Square: https://www.researchsquare.com/article/rs-10344997/v1 (unreviewed preprint)

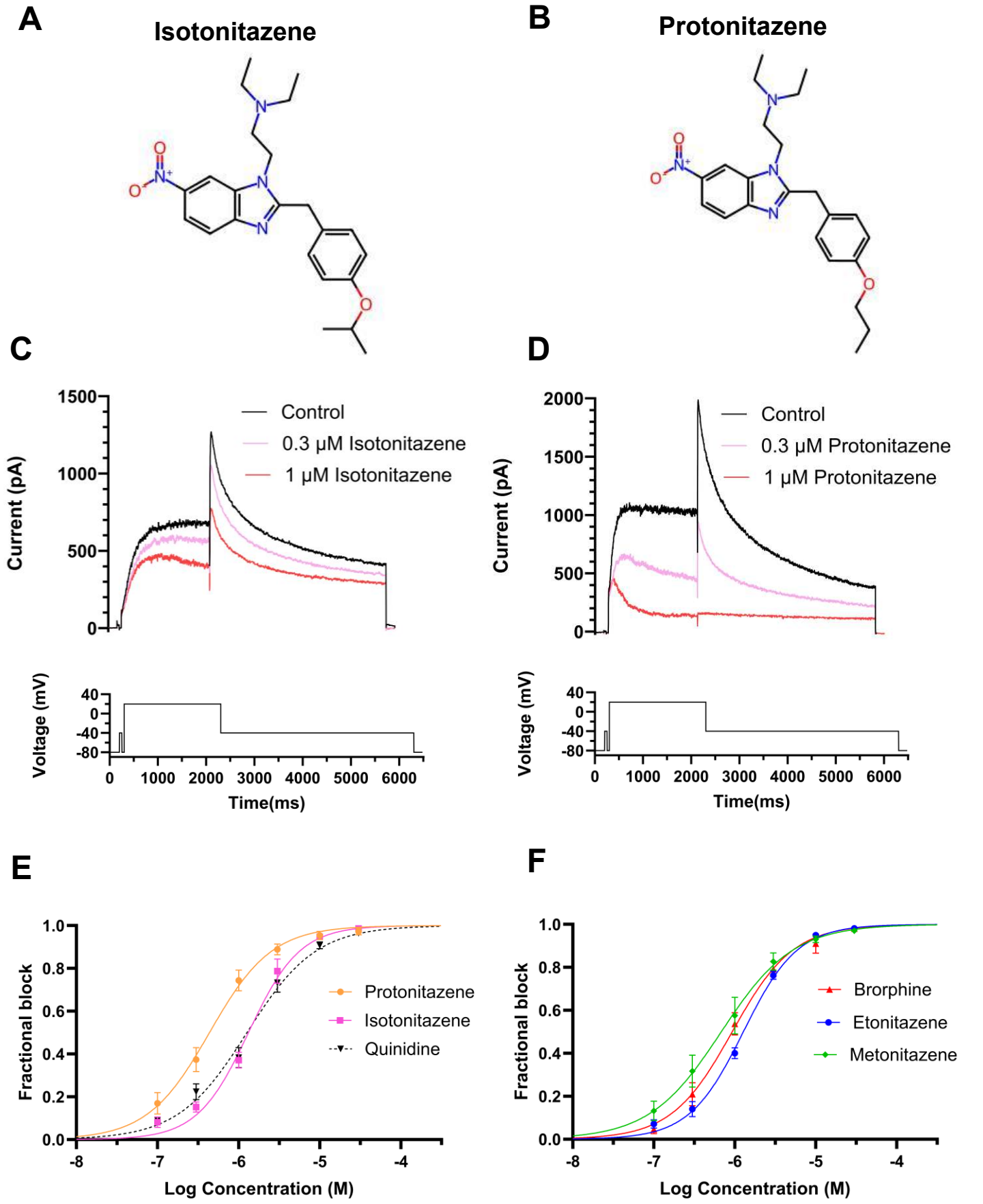
A
Isotonitazene
B
Protonitazene
C
Control
0.3 μM Isotonitazene
1 μM Isotonitazene
Current (pA)
Voltage (mV)
Time(ms)
D
Control
0.3 μM Protonitazene
1 μM Protonitazene
Current (pA)
Voltage (mV)
Time(ms)
E
Protonitazene
Isotonitazene
Quinidine
Fractional block
Log Concentration (M)
F
Brorphine
Etonitazene
Metonitazene
Fractional block
Log Concentration (M)

Figure 1

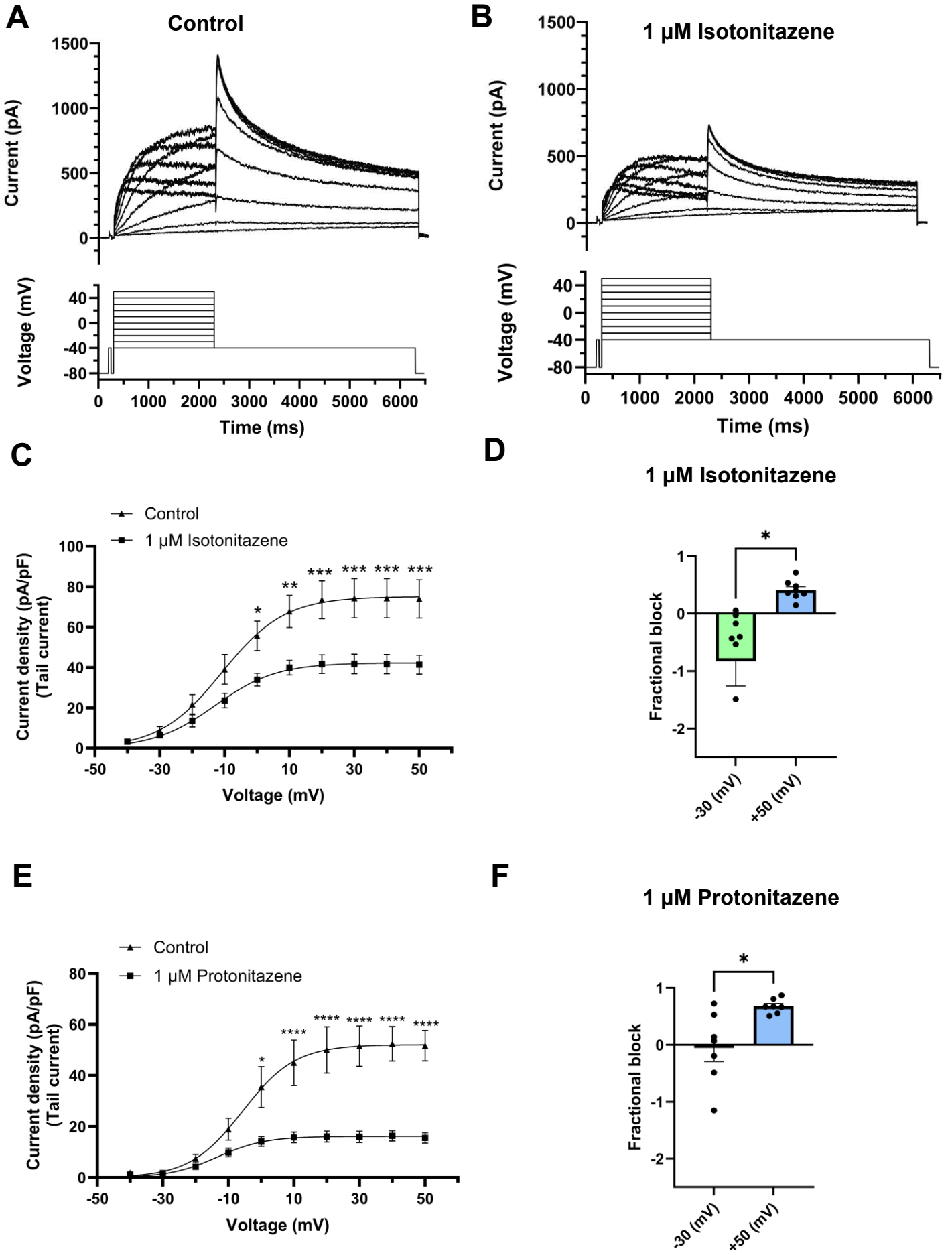
A
Control
Current (pA)
1500
1000
500
0
Voltage (mV)
40
0
-40
-80
0
1000
2000
3000
4000
5000
6000
Time (ms)
B
1 μM Isotonitazene
Current (pA)
1500
1000
500
0
Voltage (mV)
40
0
-40
-80
0
1000
2000
3000
4000
5000
6000
Time (ms)
C
Control
1 μM Isotonitazene
Current density (pA/pF)
(Tail current)
100
80
60
40
20
0
*
**
***
***
***
***
-50
-30
-10
10
30
50
Voltage (mV)
D
1 μM Isotonitazene
Fractional block
1
0
-1
-2
*
-30 (mV)
+50 (mV)
E
Control
1 μM Protonitazene
Current density (pA/pF)
(Tail current)
80
60
40
20
0
*
****
****
****
****
****
-50
-30
-10
10
30
50
Voltage (mV)
F
1 μM Protonitazene
Fractional block
1
0
-1
-2
*
-30 (mV)
+50 (mV)

Figure 2

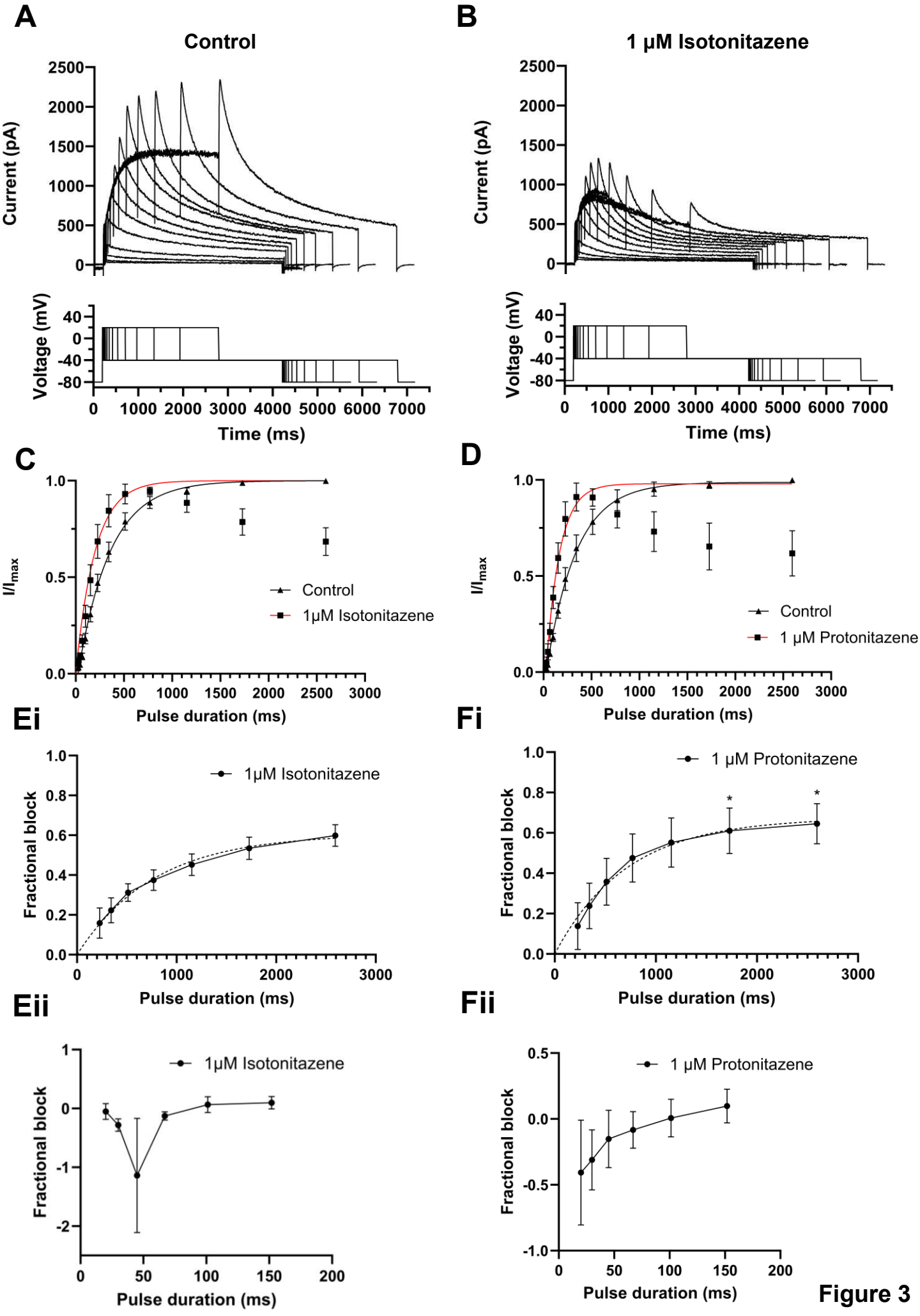
A
Control
Current (pA)
Voltage (mV)
Time (ms)
B
1 μM Isotonitazene
Current (pA)
Voltage (mV)
Time (ms)
C
I/Imax
Control
1μM Isotonitazene
Pulse duration (ms)
D
I/Imax
Control
1 μM Protonitazene
Pulse duration (ms)
Ei
Fractional block
1μM Isotonitazene
Pulse duration (ms)
Fi
Fractional block
1 μM Protonitazene
Pulse duration (ms)
Eii
Fractional block
1μM Isotonitazene
Pulse duration (ms)
Fii
Fractional block
1 μM Protonitazene
Pulse duration (ms)

Figure 3

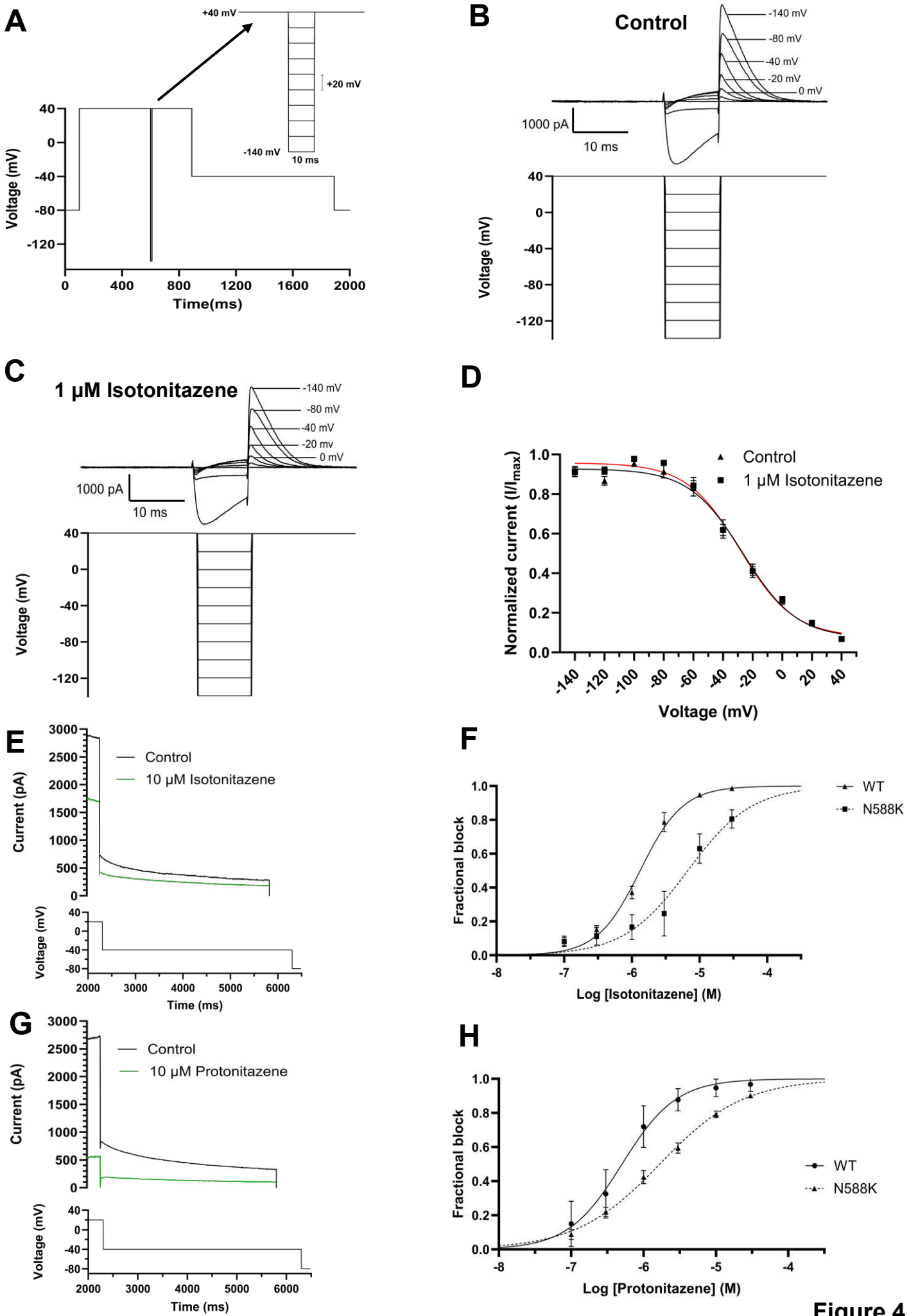
A
+40 mV
+20 mV
-140 mV
10 ms
Voltage (mV)
Time(ms)
B
Control
-140 mV
-80 mV
-40 mV
-20 mV
0 mV
1000 pA
10 ms
Voltage (mV)
C
1 μM Isotonitazene
-140 mV
-80 mV
-40 mV
-20 mv
0 mV
1000 pA
10 ms
Voltage (mV)
D
Control
1 μM Isotonitazene
Normalized current (I/Imax)
Voltage (mV)
E
Control
10 μM Isotonitazene
Current (pA)
Voltage (mV)
Time (ms)
F
WT
N588K
Fractional block
Log [Isotonitazene] (M)
G
Control
10 μM Protonitazene
Current (pA)
Voltage (mV)
Time (ms)
H
WT
N588K
Fractional block
Log [Protonitazene] (M)

Figure 4

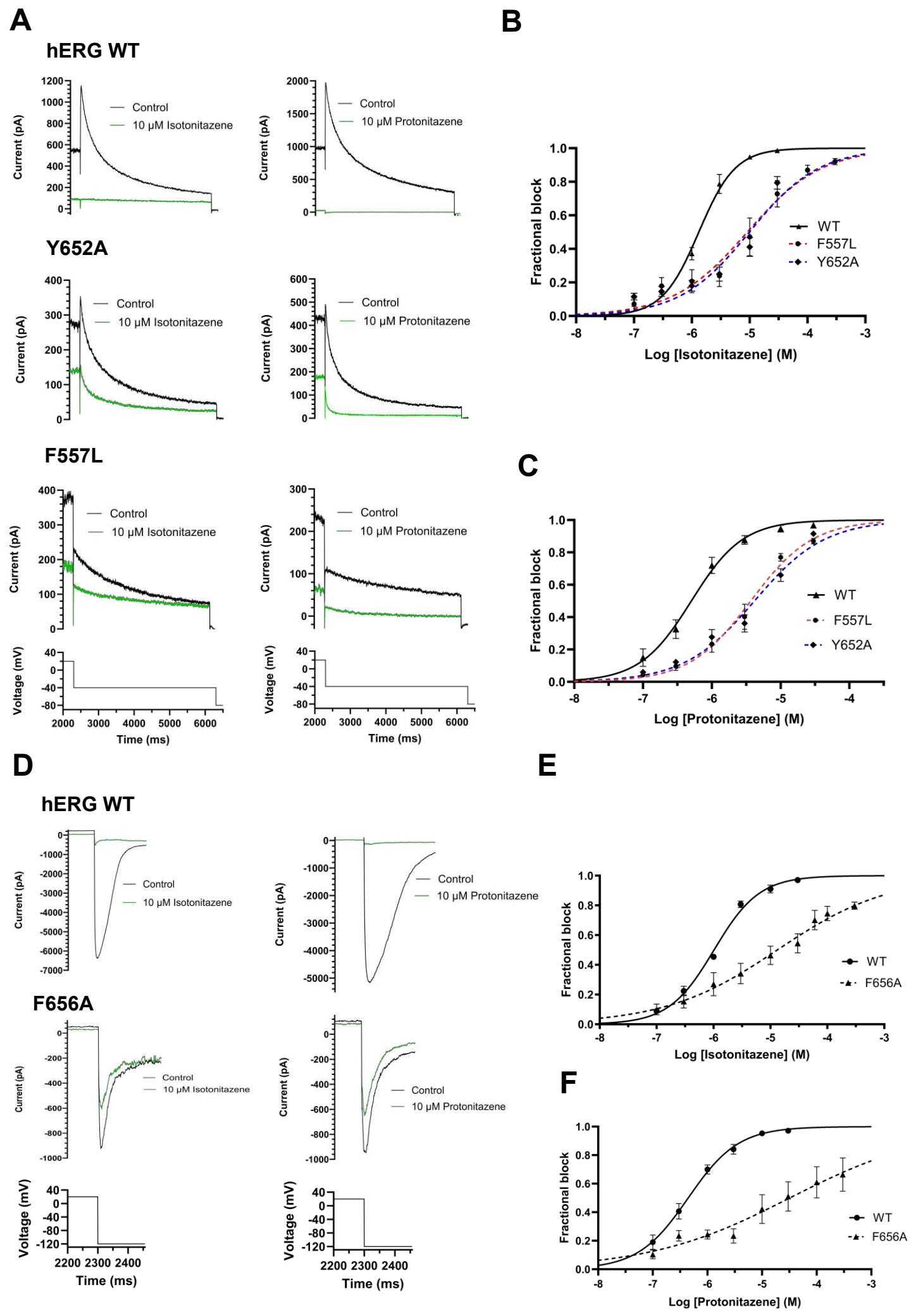
A
hERG WT
Control
10 μM Isotonitazene
10 μM Protonitazene
Current (pA)
Y652A
F557L
Voltage (mV)
Time (ms)
B
Fractional block
WT
F557L
Y652A
Log [Isotonitazene] (M)
C
Log [Protonitazene] (M)
D
F656A
E
F

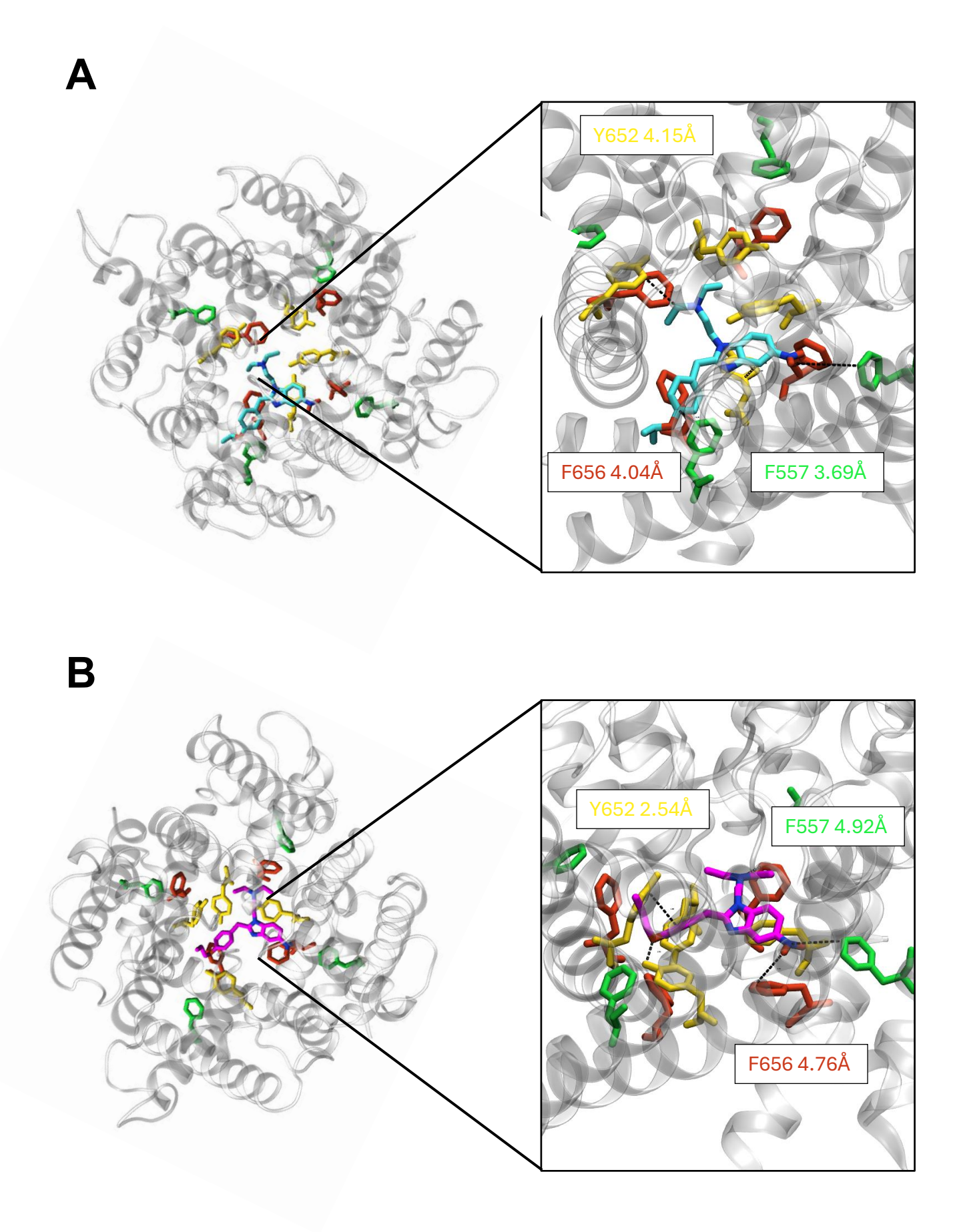
A
Y652 4.15Å
F656 4.04Å
F557 3.69Å
B
Y652 2.54Å
F557 4.92Å
F656 4.76Å

Figure 6

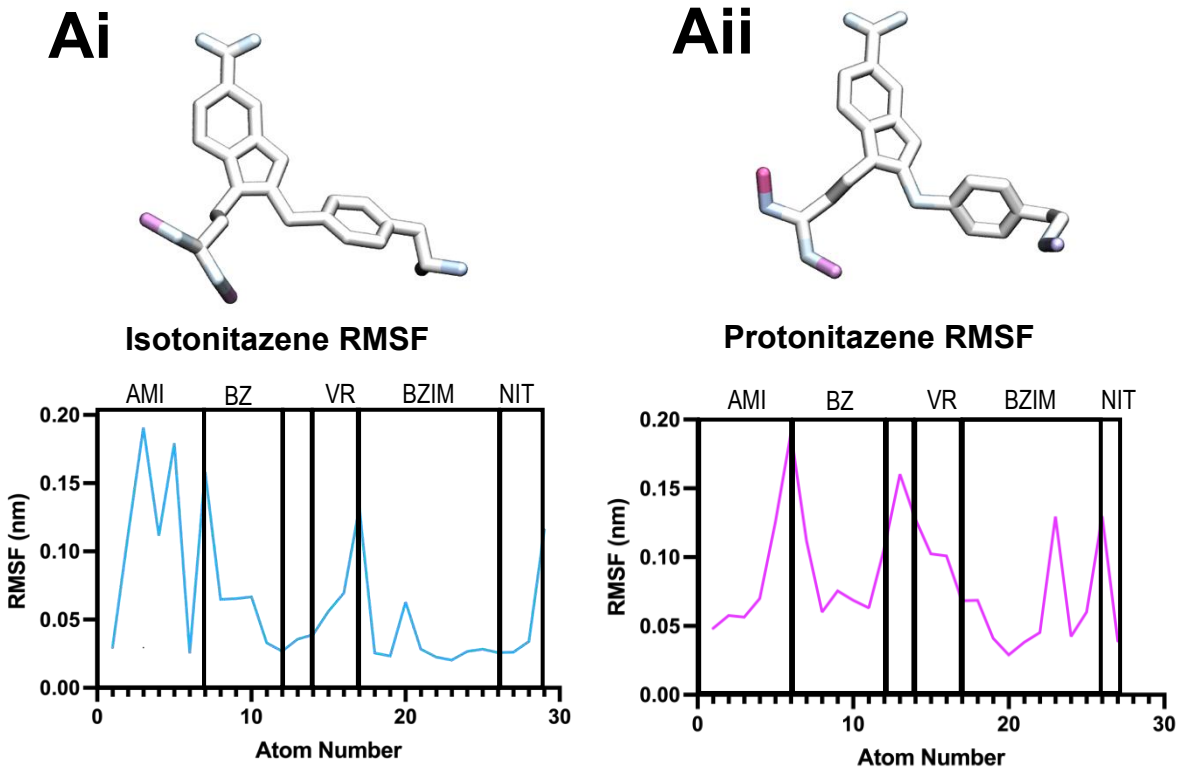
Ai
Aii
Isotonitazene RMSF
Protonitazene RMSF
AMI
BZ
VR
BZIM
NIT
RMSF (nm)
0.20
0.15
0.10
0.05
0.00
0
10
20
30
Atom Number

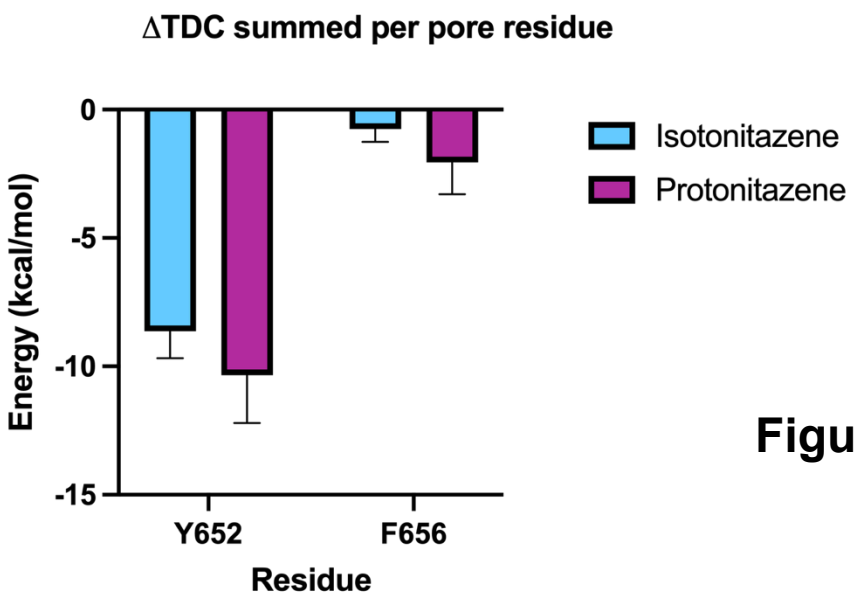
B
ΔTDC summed per pore residue
Energy (kcal/mol)
0
-5
-10
-15
Y652
F656
Residue
Isotonitazene
Protonitazene

Figure 7

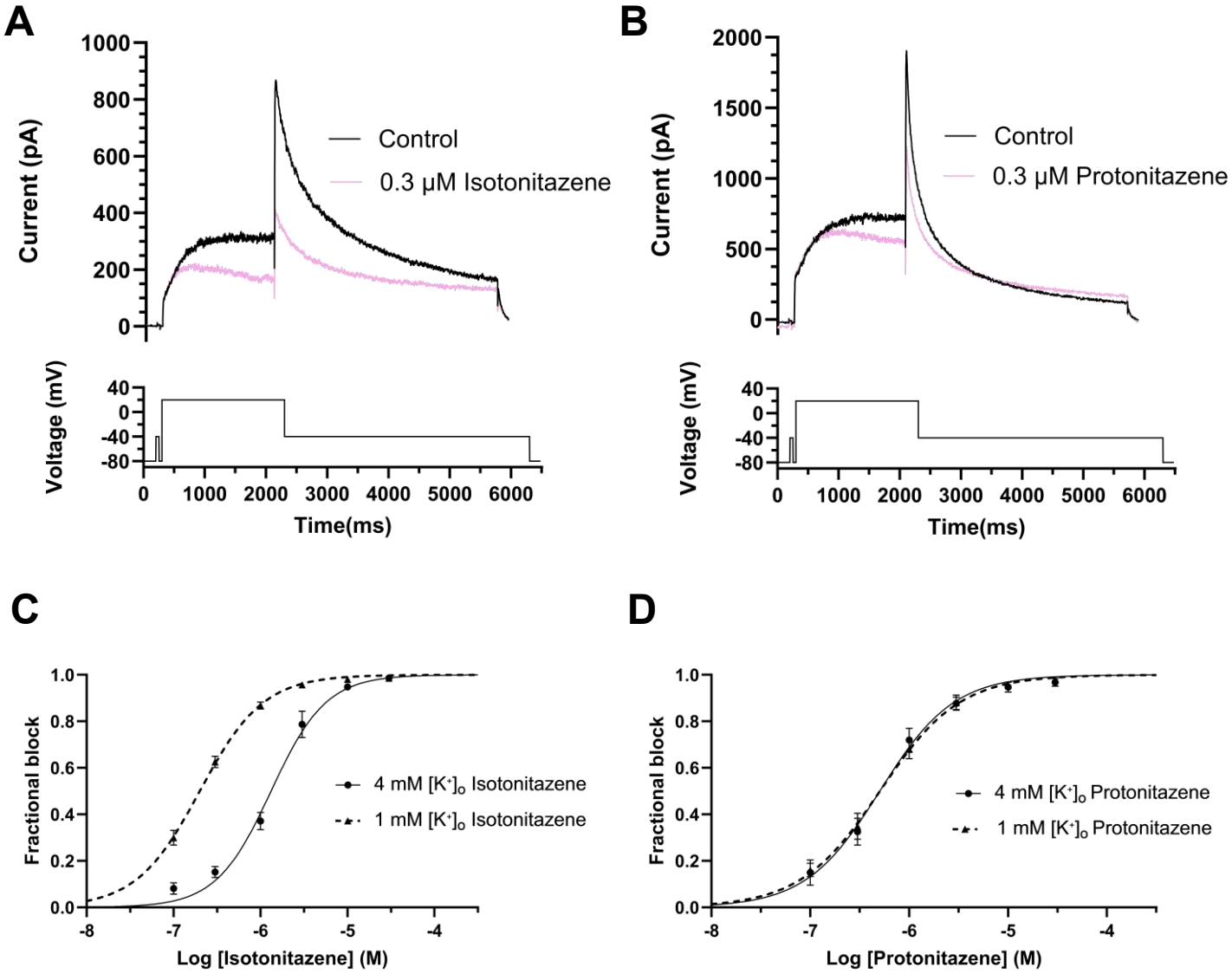
A
Current (pA)
Control
0.3 μM Isotonitazene
Voltage (mV)
Time(ms)
B
Current (pA)
Control
0.3 μM Protonitazene
Voltage (mV)
Time(ms)
C
Fractional block
4 mM [K+]o Isotonitazene
1 mM [K+]o Isotonitazene
Log [Isotonitazene] (M)
D
Fractional block
4 mM [K+]o Protonitazene
1 mM [K+]o Protonitazene
Log [Protonitazene] (M)

Figure 8

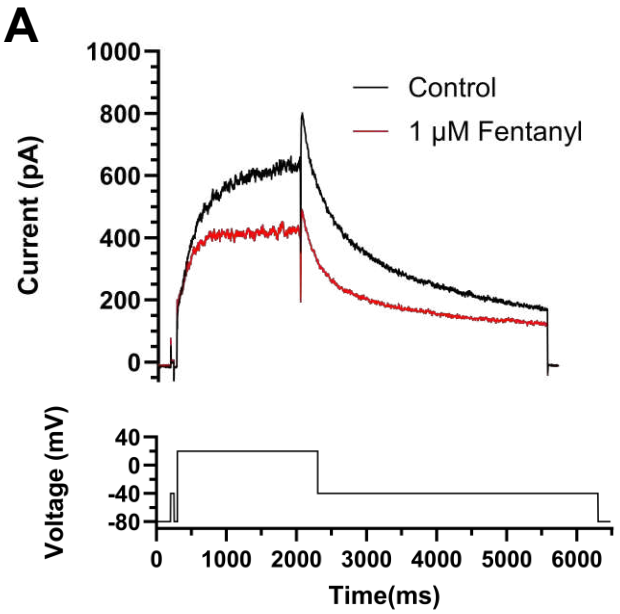
A
Control
1 μM Fentanyl
Current (pA)
Voltage (mV)
Time(ms)

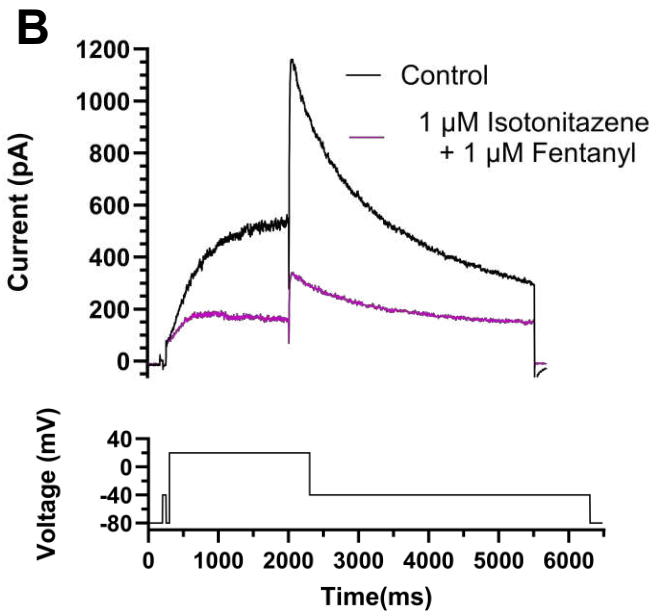
B
Control
1 μM Isotonitazene
+ 1 μM Fentanyl
Current (pA)
Voltage (mV)
Time(ms)

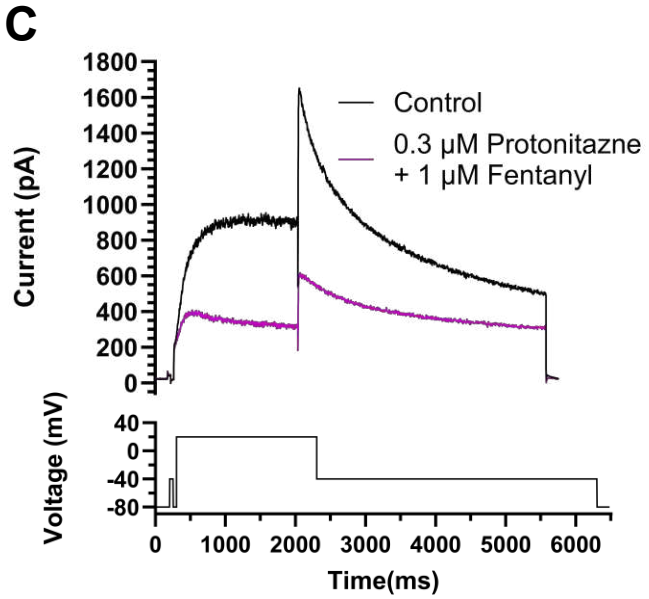
C
Control
0.3 μM Protonitazne
+ 1 μM Fentanyl
Current (pA)
Voltage (mV)
Time(ms)

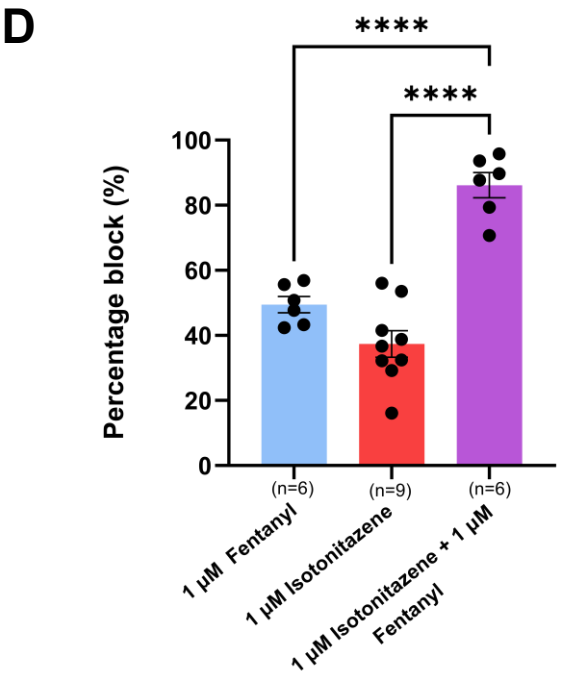
D
****
****
Percentage block (%)
(n=6)
(n=9)
(n=6)
1 μM Fentanyl
1 μM Isotonitazene
1 μM Isotonitazene + 1 μM Fentanyl

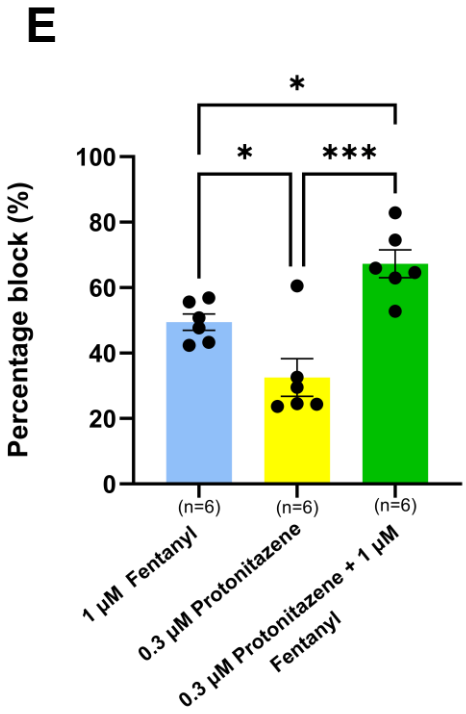
E
*
*
***
Percentage block (%)
(n=6)
(n=6)
(n=6)
1 μM Fentanyl
0.3 μM Protonitazene
0.3 μM Protonitazene + 1 μM Fentanyl

Figure 9

Supplementary Files

This is a list of supplementary files associated with this preprint. Click to download.

- NitazenehERGpapersupplementFinal.docx